BIOCHEMISTRY
including biophysical chemistry & molecular biology

Article

pubs.acs.org/biochemistry

Dynamics and Stability of the Metal Binding Domains of the Menkes ATPase and Their Interaction with Metallochaperone HAH1

Karthik Arumugam[†,§] and Serge Crouzy*[,‡]

[†]Commissariat à l'Energie Atomique/CNRS/Université Joseph Fourier, CEA, iRTSV, LCBM, 38054 Grenoble, France

[‡]Laboratoire de Chimie et Biologie des Métaux, CEA, iRTSV, LCBM, Commissariat à l'Energie Atomique/CNRS/Université Joseph Fourier, UMR 5249, 17 rue des martyrs, 38054 Grenoble Cedex 09, France

Supporting Information

ABSTRACT: Human copper-ATPases ATP7A and ATP7B are essential for intracellular copper homeostasis. The main roles of the Menkes protein, ATP7A, are the delivery of copper to the secretory pathway and the export of excess copper from the enterocytes. The N-terminal domain of membrane protein ATP7A consists of six repetitive sequences of 60−70 amino acids (Mnk1−Mnk6) that fold into individual metal binding domains (MBDs) and bind a single copper ion in the reduced Cu^{I} form via two cysteine residues. The structure of each individual MBD is known from nuclear magnetic resonance experiments. Here, we were interested in the stability and dynamics of each isolated MBD in their apo and holo forms and their interactions with the soluble metallochaperone HAH1 that delivers copper to ATP7A. Using molecular dynamics simulations of the MBDs under different conditions, we show that some MBDs (Mnk1 and Mnk5) present large root-mean-square deviations from initial structures or large root-mean-square fluctuations, and great care has to be taken in setting up the simulations. We propose that the first MBD, Mnk1, probably important in the transfer of copper between the metallochaperone and ATPase, could be stabilized by interactions with other MBDs, including a domain located in the loop between Mnk1 and Mnk2. An important result of this work is the apparent direct correlation between the difference in the fluctuations of the metal binding site loop in its apo and holo forms and the measured affinity of the MBD for copper. This difference decreases from Mnk1 to Mnk6, Mnk4, and Mnk2 in this order. The study of the exposure to the solvent of the metal and the residues of the metal binding loop of the MBDs also shows different behavior for each MBD. In particular, copper in serine-rich domain Mnk3 and largely fluctuating domain Mnk5 appears to be more solvent-exposed than in the other MBDs. In the second part of this work, we investigated the importance of electrostatics in the MBD−chaperone interactions using different docking programs. Mnk1 and Mnk4 present a large electrostatic dipole moment and large stabilizing interaction energies with HAH1. Finally, we propose a model structure of ATP7A from Mnk6 (E561) to P1413 based on the crystal structure of LpCopA and docking simulations.

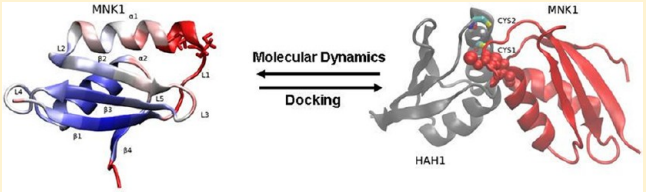

P(1B)-ATPases make up a subgroup of P-ATPases that transport heavy metals (Cu^{+}, Cu^{2+}, Zn^{2+}, Co^{2+}, Cd^{2+}, and Pb^{2+}) across biological membranes.[1] Present in most organisms, they are key elements for metal homeostasis. Among them, the human copper-ATPases ATP7A and ATP7B are essential for intracellular copper homeostasis. The copper-ATPases use the energy of ATP hydrolysis to transport copper from the cytosol into the secretory pathway and thus supply the metal for subsequent biosynthetic incorporation into various copper-dependent enzymes. ATP7A is required for the formation of functional tyrosinase,[2] peptidyl-α-monooxygenase,[3] lysyl oxidase,[4] and possibly some other enzymes.[5] In addition to their biosynthetic role, human copper-ATPases participate in the export of excess copper from the cells. The essential role of ATP7A in the export of copper from intestinal epithelium is best illustrated by the phenotype of Menkes disease. In this lethal human disorder, the functional ATP7A is lost because of various mutations in the corresponding gene, resulting in greatly impaired export of copper from the enterocytes.[6] In Menkes disease, the lack of functional copper-ATPase is also associated with the disrupted delivery of copper to the secretory pathway, and the deficiency of active copper-dependent enzymes, for example, lysyl oxidase, greatly contributes to the severity of the disease phenotype.[7] The molecular architecture of human copper-ATPase is known because of knowledge accumulated through various biochemical predictions and experiments (for a review, see ref 8). Both ATP7A and ATP7B have eight predicted transmembrane segments (TMS) that form a copper translocation pathway. The highly conserved CPC residues in TMS6 contribute to the intramembrane copper binding site(s). The transmembrane segments of copper-ATPases are connected by loops of different length, which are fairly short at the luminal side of the transporters. The bulk of copper-ATPases and their key functional domains (the N-terminal domain, the ATP binding domain, the A-domain, and the C-terminal tail) are all cytosolic. Six

Received: May 22, 2012
Revised: September 14, 2012
Published: October 17, 2012

transmembrane segments (TMS3−8) in the membrane portion of copper-ATPases have equivalents in the structure of other P-type ATPases, while the first transmembrane hairpin (TMS1,2) seems to be unique for the P1B-ATPases and is not found in other P-type pumps of known structure to date. TMS1,2 is directly linked to the large N-terminal copper binding domain via TMS1. The first structure of a bacterial copper-ATPase was released recently in the Protein Data Bank (PDB) (entry 3RFU),[9] but the N-terminal unique MBD of this ATPase was not resolved in the structure.

The N-terminal domain of human copper transporting ATPases consists of six repetitive sequences of 60−70 amino acids that are characterized by an invariant GMxCxxC motif. Each of these sequences folds into individual metal binding domains (MBDs) and binds a single copper ion in the reduced Cu^I form via two cysteine residues.

Since the time when common biochemical mechanisms among the copper-transporting P-type ATPases began to emerge,[10] the role of individual MBDs in the metal-dependent targeting and localization of these proteins has been precise.[1] In vivo, MBDs receive Cu^I from the corresponding copper chaperones, HAH1 (also known as Atox1) in the case of ATP7A. Their metal selectivity appears to be determined, in part, by the specific MBD−chaperone interaction via electrostatic and hydrophobic interactions.[1] Several studies have made it clear that in both the Menkes and Wilson disease proteins, not all the metal binding repeats are needed to allow transport activity.[11] ATP7A is localized preferentially at the trans-Golgi network (TGN). At a high Cu^IHAH1:Mnk1−6 ratio, the Cu^I-bridged adduct between HAH1 and domains 1 and 4 could accumulate and interact with ATPase domain A, affecting the balance between ATP7A phosphorylation and dephosphorylation in a way such that ATP7A would become preferentially localized at the plasma membrane.[12]

Mnk3 of ATP7A is poorly metalated by Cu^IHAH1 in solution, and at high Cu^IHAH1:Mnk1−6 ratios, domains 2 and 3 essentially do not seem to interact with Cu^IHAH1 and are not metalated.[12] At all metal concentrations, copper translocation would occur through domains 5 and 6.[12] Studies have shown that at least one of the C-terminal-most metal binding domains (Mnk5 or Mnk6) is needed to allow the copper-induced translocation of the ATPase[13] and that the first four metal repeats, Mnk1−4, could be eliminated without a loss of copper-induced relocation. When presented to the entire N-terminal tail (Mnk1−6), Cu^IHAH1 showed, in solution, the formation of detectable amounts of a macromolecular complex with both domains 1 and 4, whereas domain 6 was able to remove Cu^I from the metallochaperone.[12] Presented with Mnk4−6 of ATP7A, only, HAH1 demonstrated a preference for donating copper to domain 4,[14] although domains 5 and 6 of ATP7A can also accept copper from copper-HAH1. The presence of Mnk5 and Mnk6 seems to influence the affinity of the intramembrane copper binding site(s), most likely by shifting the E1−E2 equilibrium upon copper binding and/or dissociation. Moreover, the loops connecting N-terminal MBDs vary in length, but the linker between domains 4 and 5 in the N-terminal domain of ATP7A is much longer than that between domains 5 and 6. This observation and the presence of only one or two MBDs in bacterial copper-ATPase suggest that Mnk5,6 may represent an autonomous subdomain within the N-terminus of copper-ATPases.[8]

Today, the precise role of each MBD still remains a point of great interest with no clear answer. The availability of the structure of each MBD has allowed atomic studies of the relations between their structure and function (see, for instance, refs 1, 15, and 16). Each domain consists of four β-strands and two α-helices folded into a stable $\beta\alpha\beta\beta\alpha\beta$ "ferredoxin-like" structure.

Given their structure, molecular dynamics (MD) simulations are a perfect tool to shed new light on the different behavior of individual MBDs. Simulations allow the study of the stability of the domains in both their apo and holo forms; they are also useful for seeing the orientation of the cysteine residues and their more or less important exposure to the solvent that can be a key factor in metal binding and transfer.[17] The dynamics of HAH1, the metallochaperone that delivers copper to the MBDs, was studied in a previous work.[18] Here, we were interested in the stability and dynamics of each isolated MBD. In our simulations, some MBDs were slightly unstable, losing part of their secondary structure, and we decided to introduce light harmonic distance restraints between H-bonded atom pairs. The exposure to the solvent of the residues of the metal binding loop of the MBDs has also been studied. We will show that atom root-mean-square deviations (rmsds) and root-mean-square fluctuations (rmsfs) during MD simulations help us to understand the role of each MBD, especially domains 1 and 4−6.

In the second part of this work, we investigated the importance of electrostatics in the MBD−chaperone interactions using different easily accessible docking programs. Although a consensus result between the programs is difficult to obtain, we tested them on the known structure of the complex between domain 1 and HAH1.[19] Setting as a condition for a good docking the proximity of the MBS of each partner, we propose models of the complexes between domains 1, 2, 4, and 5 and HAH1. Following the same idea, we propose a model structure of ATP7A from E561 to P1413 by docking of holo Mnk6 on a model structure of the ATPase core obtained by Gourdon et al.[20] from the known structure of the Cu^I-ATPase from *Legionella pneumophila* (LpCopA).[9] Although the distance between Cu^I and the putative entry residues for copper transport is short, the problem of copper-mediated translocation of the ATPase, far beyond the possibilities of current modeling, was not addressed.

In conclusion, we propose a reinterpretation of some experimental results on the Menkes MBD−HAH1 interactions in light of our modeling.

MATERIALS AND METHODS

Starting Structures and Models. All MD simulations were performed with CHARMM[21] (version c35b2) using the charmm27 all-atom force field.[22] To cope with the lack of parameters for metals in the CHARMM force field, researchers in our team developed, in a previous work,[23] special parameters for Cu^I bound to cysteine sulfur atoms in proteins, in a fixed linear geometry. In our model, the transfer of charge between thiolate and metal is approximated by a covalent bond between metal and sulfur. The electrostatic field around the metal accurately reproduces ab initio calculations by a careful adjustment of partial atomic charges of thiolates and metals.

Three-dimensional atom coordinates of the Menkes metal binding domains (MBDs) were obtained from the nuclear magnetic resonance (NMR) structures from the Protein Data Bank (PDB) entries given in Table 1.

Because the MBDs of the Menkes ATPase are part of a longer protein, N- and C-terminal residues have been capped

Table 1. List of Menkes Metal Binding Domains Used in the Simulations[a]

		apo		holo	
	sequence	PDB entry	rmsd (Å)	PDB entry	rmsd (Å)
Mnk1	G6−D79	1KVI[24]	1.8	1KVJ	2.0
Mnk2	G169−K240	1S6O[25]	1.3	1S6U	1.2
Mnk3	N275−T348	2G9O[26]	1.0	2GA7	1.2
Mnk4	L375−D446	1AW0[27]	1.0	2AW0	1.0
Mnk5	N486−N558	1Y3K[16]	1.7	1Y3J	2.4
Mnk6	D563−K633	1YJU[28]	1.6	1YJV	1.6

[a]PDB entries of the NMR structures are given. The rmsds of the Cα atom coordinates of the 10 models found in each PDB entry are given.

with a neutral acetylated N-terminus and an amidated C-terminus, respectively (ACE and CT2 as defined in the CHARMM topology file).

The first model of each of the solution structure PDB files of the proteins was used as a starting conformation for all MD simulations (models are structurally very close, and this choice is likely to have no influence on the results reported here). Counterions (chloride or sodium) were added to the systems when necessary to keep them electrically neutral (they were initially placed to minimize their electrostatic interaction with the protein).

Proteins were solvated with TIP3P water molecules[29] in an orthorhombic box. Water molecules with an oxygen atom <2.4 Å from any protein heavy atom (i.e., non-hydrogen atom) were deleted.

Details of the MD Simulation. The systems were energy-minimized, and the protein heavy atoms were first constrained with a harmonic force constant of 1 kcal mol^{-1} Å^{-2} for 5 ps MD simulations. Then, it was decreased to zero in 0.2 kcal mol^{-1} Å^{-2} steps every 5 ps. The systems were equilibrated for 30 ps at a constant temperature (300 K) with periodic boundary conditions, and using the particle mesh Ewald method[30] for calculation of long-range electrostatic interactions. Langevin dynamics with a friction coefficient of 3 ps^{-1} for all protein non-hydrogen atoms was used.

After the 30 ps equilibration, the temperature of the system was kept at 300 K with a Nosé-Hoover thermostat and the pressure was maintained around 1 atm with a Langevin piston. The area of the system was kept constant (NPAT ensemble) in the Y and Z directions, while the X dimension (and thus the volume) was allowed to vary. The pressure was adjusted through the CPT module in CHARMM and a piston mass of 750 amu in the X direction. SHAKE[31] was used to constrain all covalent bonds involving hydrogen atoms at their equilibrium length. All the simulations employed the leapfrog Verlet algorithm with a 2 fs integration time step and consisted of 20−30 ns production dynamics (after the 30 ps equilibration MD described above). Simulations of metal binding domain i will be noted Mnk$i$ in the following. For all Mnk systems, the variable box dimension was rapidly equilibrated with very small standard deviations of ∼0.05 Å.

The simulations were analyzed over the last 15 ns. The criteria used to determine the convergence of the simulations were the total and potential energy terms, the crystal dimensions, and the time evolution of the secondary structure elements, and of the rmsd of the backbone atom position with respect to the corresponding experimentally resolved starting conformation.

Average structures of the six Mnk systems in their apo and holo forms were calculated from the last 15 ns of the MD trajectories. Harmonic restraints of 1 kcal mol^{-1} Å^{-2} were applied on all non-hydrogen atoms, and then the average structures were energy-minimized using 200 steps of steepest descent followed by ABNR minimization down to a gradient of 0.1 kcal/mol.

Restraints. *Initial Restraints.* Simulations were conducted in the presence of four mild distance restraints aimed at preventing the "opening" (fraying) of the structures between β-strands. These restraints of the type "biharmonic with well" are treated as "NOE-like" restraints in CHARMM and have the following form:

$$E_{\mathrm{NOE}} = \sum_{\mathrm{restraints},r} k_r \Delta^2$$

with

$$\Delta = \begin{cases} R - (d + d_{\mathrm{plus}}) & \text{if } d + d_{\mathrm{plus}} < R \\ 0 & \text{if } d - d_{\mathrm{minus}} < R < d + d_{\mathrm{plus}} \\ d - d_{\mathrm{minus}} - R & \text{if } R < d - d_{\mathrm{minus}} \end{cases}$$

where the distance between the two atoms is R, the target distance is d, and the restraining potential is null for $d - d_{\mathrm{minus}} < R < d + d_{\mathrm{plus}}$. The following values were used: k_r = 20 kcal mol^{-1} Å^{-2}, d = 2.0 Å, and $d_{\mathrm{minus}} = d_{\mathrm{plus}}$ = 0.2 Å. These restraints correspond to hydrogen bonds between atom O/H of one residue in β1 and atom H/O of one residue in β4 and between atom O/H of one residue in β2 and atom H/O of one residue in β3.

Additional Sessions and Restraints. As already explained, all Mnk MBD systems were first simulated for ≥20 ns with four mild NOE-type restraints aimed at preventing fraying of the β-strands (simulations termed session 1 hereafter). After initial analysis of these results, we noticed a large coordinate rmsd with respect to initial NMR structures and loss of secondary structure elements for several systems. We then decided to run an additional MD session (called session 2) in which we would add distance restraints of the type described above but with smaller force constants (k_r = 2 kcal mol^{-1} Å^{-2}) to maintain all backbone H-bonds found in the NMR PDB structure.

Docking Simulations. Following the common idea that metallochaperone and ATPase MBDs initially interact via electrostatic interactions,[19,32] we considered the two partners as two dipoles with non-zero charge at long distances. We set up and ran test dockings with CHARMM in which we would control the initial position of the two partners after orienting them to maximize their dipolar interactions. Then, we performed docking simulations using seven standard docking programs. The idea was to position the two proteins to maximize their potential electrostatic interaction and let them come in contact under the effect of nonbonded forces supplemented with a distance restraint force to accelerate the interaction (CHARMM docking).

Finally, standard protein protein docking programs have been used to try solve the same problem of the preferred interactions between HAH1 and the MBDs.

Initial structures for the dockings were taken from the NMR structures of the apo MBDs and holo HAH1. In an additional

dx.doi.org/10.1021/bi300669e | Biochemistry 2012, 51, 8885−8906

docking simulation named Mnk1HAH1, the structures of HAH1 and Mnk1 were those found in the NMR complex[19] (PDB entry 2K1R) with little change: the coordinates of Met 1 were removed, and the coordinates of Pro 74 and Asp 75 were built from internal coordinates to fit the Mnk1 sequence in PDB entry 1KVI. In this way, the simulations run starting from the separated structures: Mnk1 from PDB entry 1KVI and HAH1 from PDB entry 1TL4 and from the structures of the two partners in the complex from PDB entry 2K1R were comparable (same number of atoms). The structures were energy-minimized using the CHARMM19 (toph19, param19) united atom force field from the structure of HAH1 and Mnk1 found in the NMR complex[19] (PDB entry 2K1R) with ABNR minimization down to a gradient of 0.1 kcal mol^{-1} $Å^{-1}$. Minimizations were done in vacuum with strong harmonic restraints to the initial structure (force constant of 5 kcal mol^{-1} $Å^{-2}$) to have "standard" comparable input structures for all programs. Finally, these structures were centered at the origin and oriented to align their principal axes with the coordinate system.

Docking with CHARMM. A new protocol with CHARMM allowing the fine control of the initial interaction of the two partners was devised. We ran short MD simulations to force the two partners, HAH1 and each Menkes MBD, to diffuse toward each other because of their long-range electrostatics interaction to bring the cysteines of the metal binding sites (MBSs) sufficiently close for potential copper transfer.

HAH1 (with bound Cu^{I}) and the six MBDs were reoriented so that their dipole moment lies on the $+X$ direction (same direction and same sense): then the molecules were rotated around X to align either the copper atom (HAH1) or the midpoint between the S atoms of metal binding cysteines on the Y axis (oriented dipole configurations). Then when the CHARMM docking simulation was started, the two proteins were placed 30 Å from each other along the X axis and HAH1 (with bound copper) was slowly translated toward Mnk in steps of 0.25 Å, keeping maximal dipolar interaction. In practice, HAH1 was translated, backbone atoms of the two proteins were fixed, and the complex was energy-minimized (ABNR down to a gradient of <0.1 kcal mol^{-1} $Å^{-1}$). Langevin dynamics (4 ps) at 300 K were run followed by a new minimization down to a gradient of 0.01 kcal mol^{-1} $Å^{-1}$. Energies were calculated in vacuum using a nonbonded cutoff of 13 Å and the atom FSHIFT, VSHIFT cutoff schemes. Then a new translation step was done until the interaction energy between HAH1 and Mnk became positive because of van der Waals contacts between backbone atoms. Again, energy minimizations and dynamics were run in vacuum using the CHARMM19 force field, and the structure with the lowest interaction energy (after freeing up all atoms) was kept for the following step.

At that point, the two partners were close to each other with aligned dipoles so that their interaction energy was maximal (and negative) (stage 1). Copper was removed from the structure to allow comparison with standard docking programs that are not parametrized for metals. Depending on the MBD, the distance between the midpoints of the two MBS cysteine sulfur atoms of the two proteins, δSS, varied between 11.5 (Mnk2) and 37.9 Å (Mnk6). Then, the proteins were allowed to reorient in rotation and forced to present their MBS cysteine in closer contact (as if ready for copper exchange). A harmonic distance restraint on δSS acting for a δSS of $\geq$10.0 Å with a force constant of 2 kcal mol^{-1} $Å^{-2}$ was applied. Large distance restraints (force constant of 20 kcal mol^{-1} $Å^{-2}$, similar to those described previously for session 2 simulations) were applied to maintain the secondary structures of the two proteins. Starting from stage 1, short minimizations were run followed by 200 ps Langevin MD simulations at 300 K. Simulations were conducted in vacuum with a nonbonded cutoff of 13 Å (FSHIFT, VSHIFT option). The distance restraint on δSS was changed to act for a δSS of $\geq$5.0 Å with a force constant of 5 kcal mol^{-1} $Å^{-2}$, and a new 200 ps Langevin MD simulation was run. In the last step, the distance restraint on δSS was again changed to act for a δSS of $\geq$4.8 Å with a force constant of 10.0 kcal mol^{-1} $Å^{-2}$ and a final 1 ns Langevin MD simulation was run. At the end, structures were energy-minimized (ABNR) down to a gradient of 0.02 kcal mol^{-1} $Å^{-1}$ (stage 2). Finally, to check the stability of the obtained complexes, new simulations were run, starting from stage 2 and after removing the restraint on δSS (but keeping the secondary structure restraints). Additional 1 ns Langevin MD simulations were performed followed by energy minimization down to a gradient of 0.02 kcal mol^{-1} $Å^{-1}$. A nonbonded cutoff of 13 Å and the recommended atom FSWITCH, VSHIFT cutoff schemes (more precise but more expensive than the FSHIFT option used above) were used in this last stage (stage 3).

Docking with Several Docking Programs. Starting from the initial coordinates obtained after Docking Simulations, we removed the copper atom from the structure of HAH1 because it is, in general, not accepted by the docking programs. Then, the seven following docking programs were used.

Docking was run through the Haddock Web server[33] with Haddock version 2.0. The four amino acids, including the metal binding cysteines (CxxC), of each protein were defined as active residues.

HEX[34] version 6.1 was used for the docking with and without electrostatic components in the scoring and with full MM final refinement (docking_refine = 3). The receptor and ligand angle ranges were set to 40°, and the translation range was set to 40 Å in steps of 0.75 Å. All other parameters of the program were the default parameters. The model with the lowest total energy ($E_{total} = E_{shape} + E_{force}$) was kept.

ClusPro version 2.0 (http://cluspro.bu.edu/home.php) was used[35] with the "Electrostatic-favored" option. The lowest-energy model was kept.

ZDOCK version 3.0.2 (http://zdock.umassmed.edu/) was used.[36] The docking was directed by selecting residues to force into the binding site: the four CxxC residues of both HAH1 and the Menkes MBDs. The first model complex was kept.

ATTRACT (Python edition) version 0.3[37] was used, as implemented on a local workstation with default parameters. Again, the lowest-energy model was retained.

PatchDock (http://bioinfo3d.cs.tau.ac.il/PatchDock/)[38] was used. The docking was directed by selecting receptor and ligand sites: the four CxxC residues of both HAH1 and the Menkes MBDs. The model with the highest score was kept.

GRAMM-X (http://vakser.bioinformatics.ku.edu/resources/gramm/grammx)[39] was used. The four CxxC residues of both HAH1 and the Menkes MBDs were considered as interface residues; two residues in the interface and one receptor−ligand residue pair were required. Model 1 in the result of the server was used.

RESULTS

Sequence Alignment. A sequence alignment of metallochaperone HAH1 and Menkes MBDs Mnk1−6 used in this

work is shown in Figure 1. The alignment was done with CLUSTALW.[40] Conserved sequences in all MBDs include the

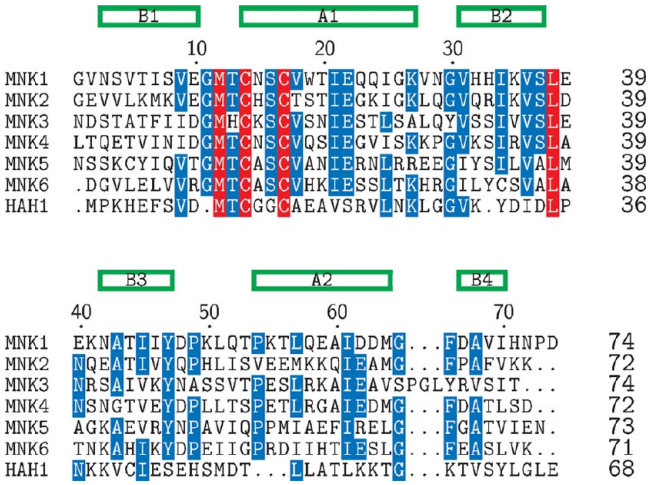

Figure 1. Sequence alignment of metallochaperone HAH1 and the Menkes MBDs Mnk1−6 used in the MD simulations. Secondary structure labeling (A for α and B for β) corresponds to the sequence of Mnk4 apo. This figure was drawn with TexShade.[41]

GMxCxSC (where x represents any residue) metal binding motif in loop L1, I21 and E22 in helix α1, V36 and L38 in strand β2, Y47 in strand β3, and I61 in helix α2. Clearly, Mnk3 presents the sequence that shows largest variability compared to others. Mnk3 lacks T13, a positively charged amino acid at position 27, G30, F49, G65, F66, and A68. An interesting observation is the number of serines in the sequences of the MBDs and HAH1 [Mnk3 (14) > Mnk4 (8) > Mnk1 = Mnk6 (6) > HAH1 (5) > Mnk2 = Mnk5 (4)], and thus, there is an outstandingly high proportion of serine residues in the sequence of Mnk3. Although it shares the same fold, HAH1 presents important differences in its sequence compared to the Menkes MBDs: it lacks the conserved G11, S16, I21, E22, and V36 residues and also the aromatic residue at position 66.

Time Evolution of Energy during Production MD. A rapid evaluation of the total potential energy of the most fluctuating system, Mnk1 apo, gives potential energies of −23853 and −23838 kcal/mol, averaged from 4 to 30 ns and from 4 to 5 ns respectively, with standard deviations of 79 kcal/mol. Thus, we estimate that energy was correctly equilibrated for all systems after a 4 ns MD simulation. Standard deviations of the total CHARMM potential energy are similar for all systems. The initial average restraining energy is negligible (0.2 kcal/mol) for all Menkes MBDs in session 1. This value increases to averages between 6 and 11 kcal/mol in simulations from session 2, where we have constrained all backbone H-bond distances. These restraining energies remain small compared to calculated average total potential energies of around −20000 kcal/mol.

Root-Mean-Square Deviations during MD. *Preliminary Simulations of the Apo Form.* A quantitative analysis of the rmsd from initial NMR structures during 20 ns MD runs (session 1) for apo Mnk systems is given in column 2 of Table 2 (the corresponding figure can be found in Figure S1 of the Supporting Information). Only Mnk6 shows low rmsds of around 1.6 Å from its NMR structure. Recently, Kouza et al. studied the effect of the Ala 629 (A67 in our notation) to Pro mutation in Mnk6 and also showed a high stability of the wild-type Mnk6 domain with contacts of the N-terminal residues with the C-terminal residues, stabilizing the end-to-end β-sheet. The five other MBDs depart significantly from the NMR structures with a maximal average deviation of 3.4 Å for Mnk1 and 3.3 Å for Mnk4. This high value agrees for Mnk1 with the large experimental rmsd between models observed in PDB entry 1KVI, but not for Mnk4 with a very low experimental rmsd (see Table 1).

Simulations of the Apo Form with H-Bond Restraints. The large rmsds from initial NMR structures obtained for some Mnk systems (especially Mnk4) motivated us to run other simulations (termed session 2) with an increased number of restraints maintaining all backbone H-bonds present in the NMR structures. An analysis of the atom coordinate rmsd from initial NMR structures during the 30 ns MD runs (session 2) for apo Mnk systems is given in columns 3 and 4 Table 2 (the corresponding figure can be found as Figure S2 of the Supporting Information). A decrease in the backbone rmsds from initial NMR structures is clearly visible compared to the results of session 1. This is especially true for Mnk4 from 3.3 to 1.0 Å, becoming the most stable of all MBDs in agreement with experimental rmsds (see Table 1), and Mnk2 from 2.6 to 1.5 Å. The rmsd of Mnk1 is only slightly reduced upon introduction of all H-bond restraints, making Mnk1 the least stable of all isolated MBDs in their apo forms. The rmsds of all atom coordinates are from 37% for Mnk1 to 125% for Mnk6 larger than those measured on backbone atoms only. The rmsds have also been calculated with respect to the centroid of the 10 NMR models of each structure. The centroid was computed

Table 2[a]

	rmsd for apo session 1	rmsd for apo session 2		rmsd for holo session 2	
system	bb (σ) (Å)	bb (σ) (Å)	total (σ) (Å)	bb (σ) (Å)	total (σ) (Å)
Mnk1	3.4 (0.24)	2.7 (0.22)	3.7 (0.18)	1.5 (0.17)	2.9 (0.14)
Mnk2	2.6 (0.17)	1.5 (0.09)	2.8 (0.08)	1.1 (0.11)	2.4 (0.10)
Mnk3	2.5 (0.18)	1.7 (0.15)	2.7 (0.16)	2.1 (0.12)	3.4 (0.13)
Mnk4	3.3 (0.33)	1.0 (0.13)	2.1 (0.16)	1.0 (0.10)	1.9 (0.11)
Mnk5	2.4 (0.20)	1.7 (0.16)	3.2 (0.11)	2.0 (0.21)	3.1 (0.20)
Mnk6	1.6 (0.12)	1.2 (0.13)	2.7 (0.14)	1.1 (0.10)	2.5 (0.09)

[a]Column 2 lists the average rmsds (standard deviation in parentheses) of backbone (bb) atom coordinates from their initial values in the NMR structures. Averages were calculated over the last 10 ns of the MD runs and for Mnk apo systems (session 1). Columns 3 and 4 list average rmsds (standard deviation in parentheses) of backbone (bb) or all (total) atom coordinates from their initial values in the NMR structures. Averages were calculated over the last 15 ns of the MD runs and for Mnk apo systems (session 2). Columns 5 and 6 list averages calculated over the last 15 ns of the MD runs for Mnk holo systems (session 2). The same analysis gives for HAH1 holo a bb rmsd of 1.4 (0.07) and a total rmsd of 2.5 (0.07).

dx.doi.org/10.1021/bi300669e | *Biochemistry* 2012, 51, 8885−8906

with the program *kclust* of the MMTSB tools.[42] No significant difference was observed compared to rmsds calculated from NMR model 1.

Preliminary Simulations of the Holo Form. Backbone atom coordinate rmsds from initial NMR structures during ≥20 ns MD runs (session 1) for holo Mnk systems were calculated (the corresponding figure can be found as Figure S3 of the Supporting Information). In their holo (Cu^{I}) forms, Mnk1, Mnk2, Mnk4, and Mnk6 show very low rmsds, meaning for Mnk1, Mnk2, and Mnk4 an important stabilization of the structures when copper is bound. High rmsds of 2.7 and 2.5 Å remain for Mnk3 and Mnk5, respectively, in agreement for the latter with the experimental rmsd between models of 2.4 Å and also with recent simulations of the fifth metal binding domain of the Wilson protein.[17]

Simulations of the Holo Form with H-Bond Restraints. As for the apo case, an additional MD session (session 2) was run for all holo Mnk systems. In this session, a clear decrease in the rmsds from 2.7 to 2.1 Å and from 2.5 to 2.0 Å (with respect to session 1) is visible for Mnk3 and Mnk5, respectively, in columns 5 and 6 of Table 2 (the corresponding figure can be found as Figure S4 of the Supporting Information). HAH1 appears to be very stable with a low rmsd from the initial structure and especially small fluctuations around the average rmsd (0.07 Å).

Thus, in their holo forms, Mnk3 and Mnk5 could be stabilized by enforcing that H-bonds defining secondary structures be conserved during the simulations.

Conservation of Secondary Structure. The stability of the different MBDs of the Menkes protein versus time during dynamics may also be easily followed through a careful study of their secondary structure elements.

Preliminary Simulations. Apo. A secondary structure analysis with Stride[43] reflects and completes the results concerning rmsds presented above. A graph of the evolution of secondary structure elements of Mnk1, in its apo form, versus time (session 1), is shown in Figure 2 (an equivalent graph for Mnk6 can be found in Figure S5 of the Supporting Information). Interesting information can be drawn from these plots. As already mentioned, Mnk6 presents a nice conservation of all its secondary structure elements at all time. Helix α1 shows instabilities in Mnk1. The α-helix changes to π- or 3−10-helices or even β-bridges. Helix α2, on the other hand, is very stable in all Mnk systems. Globally, β-strands are conserved even though they are shortened most of the time.

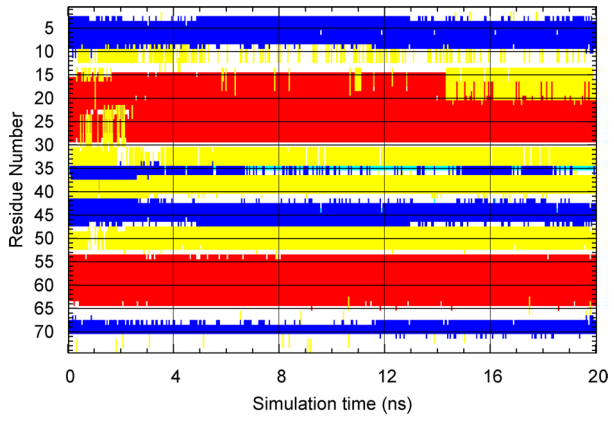

Figure 2. Evolution of secondary structure elements of Mnk1 apo with time (session 1). α-Helices are colored red, β-sheets blue, hydrogen-bonded turns yellow, 3−10-helices light red, π-helices rose, β-bridges cyan, and coils white. The $\beta\alpha\beta\beta\alpha\beta$ fold is clearly visible.

A quantitative analysis of the secondary structure elements calculated from the NMR initial coordinates and from minimized average structure for all Menkes MBDs in their apo form (session 1) has been conducted (and can be seen in Table S1 of the Supporting Information) A diminution in the number of residues in α-helices and β-strands from the NMR initial structure to the structure obtained after MD is clear for Mnk1 and compensated by a large increase in the number of turns (hydrogen-bonded turn). Mnk4 and Mnk6 appear to be very stable in terms of secondary structure. Some turns in Mnk2 are transformed into coils, and Mnk5 undergoes a dramatic disappearance of β-strands, especially β2 and β3, turning into coils or β-bridges (single pair of β-sheet hydrogen bonds).

Holo. In their holo forms, Mnk1, Mnk2, Mnk4, and Mnk6 are stable in terms of secondary structure if we except some β-strands transformed into turns for Mnk1. In Mnk2, helix α1 is noticeably longer in the Cu^{I} form both in the NMR structure[25] and after MD simulations. Noticeably, for Mnk3, an increase in the number of amino acids in α-helices and β-strands is observed after MD at the expense of turns (see Table S2 of the Supporting Information). Logically from the rmsd results, loss of structure for holo Mnk5 is observed. The number of amino acids in β-strands and turns decreases significantly, and they are replaced by coils. Strand β2 almost vanishes.

Simulations with H-Bond Restraints. After session 2 (introduction of distance restraints mimicking H-bonds), all secondary structure elements of the Mnk systems are obviously conserved, as evidenced in Figure 3 for Mnk1. In particular, helix α1 is now very stable and strand β2 regains its full length.

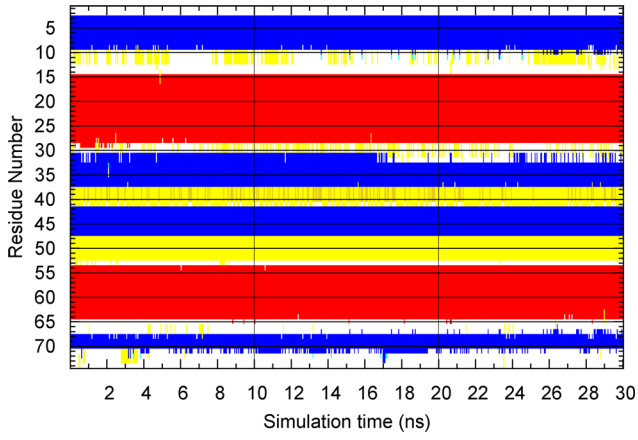

Figure 3. Evolution of secondary structure elements of Mnk1 apo with time (session 2). The color code is the same as that in Figure 2.

According to the previous data concerning coordinate rmsds and conservation of secondary structure elements with or without distance restraints, all the following results will refer to session 2 for all Mnk systems.

Root-Mean-Square Fluctuations. Root-mean-square fluctuations (rmsfs) of atom coordinates correspond to standard deviations of these coordinates around their average value in time (rmsds are averaged over several atoms or structures at a given time; rmsfs are averaged over time for a given atom or structure). Average rmsf values in the MD simulation are usually considered as good markers of the overall flexibility of

dx.doi.org/10.1021/bi300669e | *Biochemistry* 2012, 51, 8885−8906

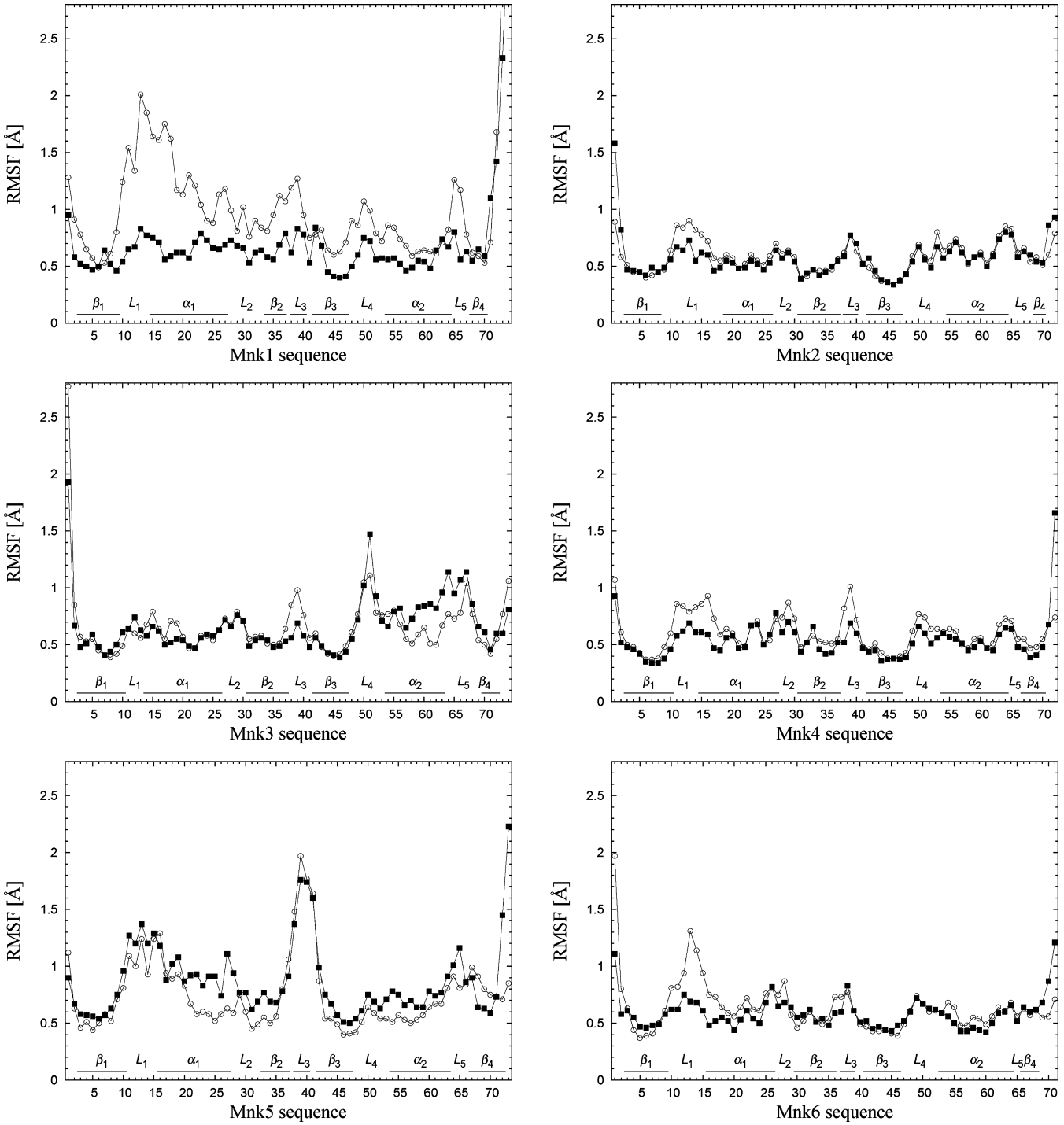

Figure 4. Root-mean-square fluctuations of the Cα atom positions of Menkes MBDs averaged over the 15 last ns of 30 ns MD simulations (session 2). Empty circles show data for the apo form and filled squares data for the Cu^{I} holo form. Secondary structure elements, as calculated with Stride from the NMR apo structure, are highlighted.

the system. The Cα atom coordinate rmsfs averaged over the last 15 ns of the MD runs are plotted in Figure 4. Logically, the residues in the α- and β-folded regions are the least mobile, with a mean rmsf of ~0.5 Å in both apo and holo forms. Large fluctuations observed in loop L1 between β1 and α1 in apo forms agree with the frequent absence of experimental NOEs in this region. A reduced mobility of residues in loop L1 around the metal binding site is observed in the holo form compared to the apo form: this is clear for Mnk1, -2, -4, and -6 and had to be expected because of the covalent bond existing between the two cysteine sulfur atoms and copper. In Mnk1 apo, this mobility of the metal binding loop is particularly pronounced. Its C-terminus is also very mobile, with residues 72−74 dangling out in water. We will propose an explanation for these apparently unrealistic fluctuations of the C-terminus in the Discussion. In the case of Mnk2, rmsf differences between apo and holo forms are visible in the cysteine-containing loop (loop 1) and the N-terminal region of the first α-helix as deduced experimentally from chemical shift variations between the two forms.[25] For Mnk5, in agreement with the imprecise definition of the two

dx.doi.org/10.1021/bi300669e | *Biochemistry* 2012, 51, 8885−8906

Table 3. rmsfs of the Cα Atom Positions of the Two Metal Binding Cysteine Residues of the CxxC Motif[a]

	HAH1	Mnk1		Mnk2		Mnk3		Mnk4		Mnk5		Mnk6	
	holo	holo	apo	holo	apo	holo	apo	holo	apo	holo	apo	holo	apo
Cys1	0.57	0.77	1.85	0.55	0.82	0.58	0.68	0.61	0.83	1.20	0.93	0.69	1.31
Cys2	0.45	0.56	1.75	0.46	0.57	0.50	0.55	0.47	0.73	0.88	0.94	0.48	0.75

[a]The rmsfs are averaged over the 15 last ns of 30 ns MD simulations (session 2).

Cu^I-binding cysteines by NMR,[16] the region around the metal binding loop shows large fluctuations both with and without bound metal. Loop L3 shows particularly large fluctuations. Mnk3 is marked by an increase in mobility of α2 and loop L5 in its holo form. Mnk2, -4, and -6 all show small rmsfs and a reduction in the mobility of loop L1 in the presence of metal. In the case of Mnk4, small rmsf differences between the apo and holo forms are concentrated in the loops, especially in the metal binding loop that is stabilized upon metal binding; this loop was also found disordered experimentally in the NMR apo structure.[27]

An analysis of the rmsfs of the two cysteines (noted Cys1 and Cys2 in the following) involved in metal binding is shown in Table 3. For all MBDs, in both their apo and holo forms (except for apo Mnk5), Cys1, the first cysteine of the consensus CxxC sequence, which always belongs to loop L1, has a higher rmsf than Cys2. This is in complete agreement with NMR results for Mnk MBDs and also for the metallochaperones apoCopZ, CuCopZ, Atx1, and HAH1, in which the first cysteine residue was found more mobile than the second (see, for instance, ref 27). We observe a significant reduction in the fluctuations of the cysteines when Cu^I is bound, again except for Cys1 of Mnk5. Mnk1 is outstanding in terms of the dynamics of the cysteines of its MBS: both cysteines show by far the largest fluctuations in their apo form and also the largest reduction of these fluctuations in its holo form. Mnk5 shows the largest fluctuations of its MBS cysteines after binding of copper with an outstanding increase in the rmsf of Cys1.

Average Atom Distributions. *Radial Distribution Function of Water around Copper.* A radial distribution function (RDF), $g(r)$, describes the probability $g(r)\ \delta r$ of finding an atom (oxygen of a water molecule) at a distance between r and $r + \delta r$ from another atom (Cu^I) as a function of the atom separation r. RDF has been widely used to study the dynamical structural modification of dense systems, to study the dynamical properties of metal ion hydration, and to search metal binding sites in proteins during MD simulations. Results of the radial distribution function of water oxygen around Cu^I are presented in Figure 5 for all Menkes MBDs, and a summary of the results is shown in Table 4. Image water molecules in the periodic images of the central simulation box have been included in the calculation of $g(r)$. A rapid inspection of the curves clearly shows that the copper ion experiences little interaction with water with very low first "shell" density for Mnk1, -2, -4, and -6; on the other hand, Mnk3 and -5 show a marked primary hydration shell around copper and HAH1 exhibits intermediate behavior. The very similar distribution of water around Cu^I for the even-numbered MBDs (Mnk2, Mnk4, and Mnk6) is remarkable and will be discussed later in light of hypotheses about a possible pairing of these MBDs. From the first peak in the radial distribution function, we observe that this first shell is located between 3.15 and 3.35 Å (x_H) from the copper ion. In this shell, a notably low number of two water molecules (N_W) hydrate the Cu^I ion in Mnk1, -2, -4, and -6. This number increases to three for Mnk3 and four for Mnk5.

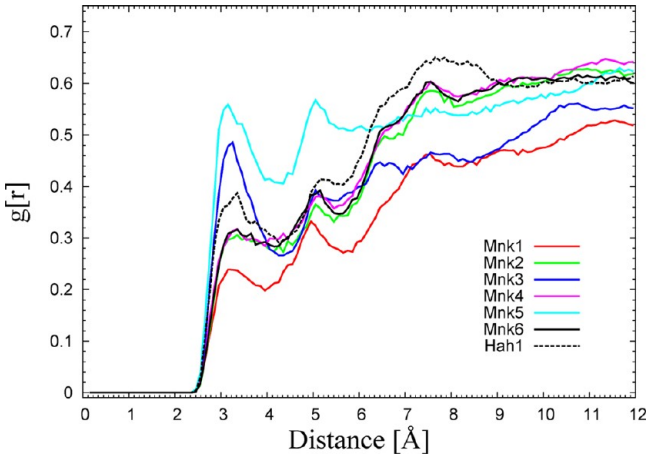

Figure 5. Radial distribution function of water around copper ion for HAH1 and all holo Mnk systems from 15 last ns of 30 ns MD runs (session 2).

Note also that, except for Mnk3, ~8 Å from Cu^I the distribution of water molecules around the ion is already that of the bulk, even more so in the case of HAH1 where bulk density is obtained at distances from copper of <7 Å.

Radial Distribution Function of Water around Protein Atoms. The radial distribution functions of water around cysteine sulfur atoms of all MBDs in their apo form are analyzed in Table 5. Cys1 and Cys2 are equally solvated in Mnk1; in Mnk3−5, Cys1 is much more solvent-exposed than Cys2, with the particular case of Mnk3, where Cys2 is completely buried with fewer than one water molecule around its S atom for distances of up to 7 Å.

In the holo form of the MBDs, both cysteines are largely exposed to the solvent with a maximal exposure for the two cysteines of Mnk5 [g_H = 1.51 at x_H = 3.15 Å for the sulfur atom of Cys2 (results not shown)]. Except for Mnk5, two water molecules belong to the first hydration shell of both cysteine sulfur atoms, fewer than in the apo case because of the implication of these atoms in the bond with copper. In the case of Mnk5, three and four water molecules are found in the first hydration shell of Cys1 and Cys2, respectively.

In the apo form of the MBDs, the side chain of methionine M12 (M11 in Mnk6) is not solvent-exposed, in general, and participates in the stabilization of the hydrophobic core[18] that consists of V9, I21, V36, and L38 (see Figure S6 of the Supporting Information). This is also the case for HAH1, in which the methionine is totally buried both in its apo and in its holo forms as can be seen from the distribution of water oxygen around the M12 sulfur atom shown in Figure 6. There is a large difference in the exposure of M12 to the solvent between apo and holo Mnk3 and Mnk5. Especially in the case of Mnk3, the Cys2 side chain originally oriented toward the hydrophobic core becomes solvent-exposed when binding copper; as a consequence, the side chain of H13, seen in only Mnk3, rotates toward the protein core and pushes away the side chain of M12,

Table 4. Analysis of Radial Distribution Functions of Water around Copper for the Holo HAH1 and Mnk Simulations from the Last 15 ns of 30 ns MD Runs (session 2)[a]

$g(r)$ data	HAH1	Mnk1	Mnk2	Mnk3	Mnk4	Mnk5	Mnk6
x_H (Å)	3.15	3.25	3.35	3.25	3.35	3.15	3.35
g_H	0.24	0.30	0.31	0.49	0.32	0.56	0.32
x_L (Å)	3.95	3.95	4.15	4.25	3.95	4.35	4.15
g_L	0.20	0.27	0.27	0.27	0.28	0.41	0.28
$\langle g \rangle$	0.51	0.59	0.62	0.55	0.63	0.60	0.61
N_W	1.3 (1.6)	1.7 (2.1)	2.1	3.0 (2.8)	1.8 (2.2)	4.2 (3.6)	2.2

[a] x_H is the distance between water oxygen and Cu^I corresponding to the first peak in $g(r)/g_H$. x_L and g_L are the distance and g values corresponding to the following minimum of $g(r)$. The position of this minimum is used as the upper bound for the integration of the first peak yielding the average number of water molecules in the first hydration sphere of Cu^I, N_W (this value is also calculated with a common upper bound of 4.15 Å for all Mnk's in parentheses). Finally, $\langle g \rangle$ is the average value (for r values between 10 and 12 Å) of the plateau reached by $g(r)$ for large r values.

Table 5. Analysis of Radial Distribution Functions of Water around Cysteine Sulfur Atoms for the Apo Mnk Simulations from the Last 15 ns of 30 ns MD Runs (session 2)[a]

	Mnk1		Mnk2		Mnk3		Mnk4		Mnk5		Mnk6	
$g(r)$ data	Cys1(S)	Cys2(S)	Cys1(S)	Cys2(S)	Cys1(S)	Cys2(S)	Cys1(S)	Cys2(S)	Cys1(S)	Cys2(S)	Cys1(S)	Cys2(S)
x_H (Å)	3.55	3.45	3.65	3.45	3.55	–	3.55	3.55	3.55	3.45	3.55	3.45
g_H	0.80	0.88	0.50	0.48	1.04	–	0.99	0.16	1.07	0.41	0.57	0.70
N_W	11	9	8	5	11	0	13	2	13	5	8	6

[a] x_H is the distance between the water oxygen and cysteine sulfur atom corresponding to the first peak in $g(r)/g_H$. N_W is the average number of water molecules in the first hydration sphere of these S atoms (integrated for $r \leq 5.5$ Å). Cys2 in Mnk3 is completely buried so that no peak appears in $g(r)$.

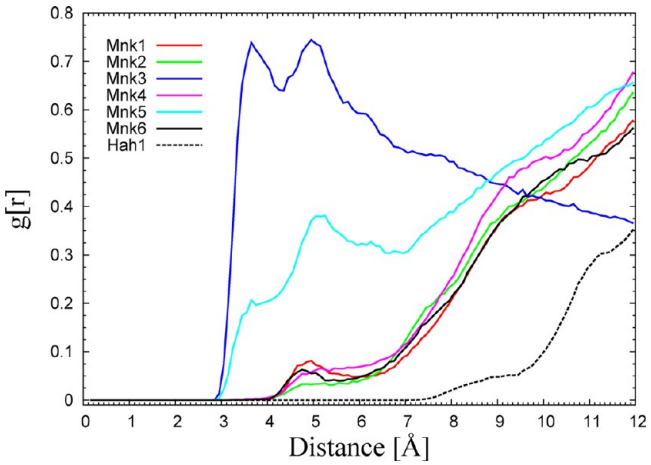

Figure 6. Radial distribution function of water around methionine M12 for all holo Mnk systems and HAH1 from the 15 last ns of 30 ns MD runs.

which becomes solvent-exposed. For Mnk1, Mnk2, Mnk4, and Mnk6, the methionine is almost completely buried, in our results, whereas in the case of Mnk5 holo, M12 points toward the solvent and I61 takes its place in the stabilization of the hydrophobic core.

Distances between Protein Atoms of the MBS. The average distances between heavy atoms close to the metal binding site were analyzed, and the results are listed in Table 6 for apo MBDs and summarized below. The side chain of F66 (or Y69 for Mnk3) is close to Cys2 for Mnk2−4 apo. The side chain of T13 is close to Cys1 in Mnk1 and Mnk2. The distance between S16(Oγ) and Cys2(S) fluctuates greatly, especially in the case of Mnk1 and Mnk4. Very small fluctuations, on the other hand, between distances monitored in Table 6 are observed in the case of Mnk3. The average distance between the sulfur atoms of the two cysteines is around 5 Å for Mnk1 and Mnk2, a distance significantly smaller than for the other MBDs. For Mnk4 apo, the cysteine side chains of the MBS are oriented in opposite directions, which is the reason for the observed large distances in Table 6. F66(Cζ), on the other hand, is very close to Cys2(S).

Structural changes that accompany copper binding are found in the metal binding loop and surrounding regions (see the detailed results in Table S3 of the Supporting Information). In our model of the MBS, copper is covalently and linearly bonded to the sulfur atoms of Cys1 and Cys2.[23] The average S−Cu^I distance is 2.1 Å, and the average Cys1(S)−Cu^I−Cys2(S) angle is 171° (rmsd of 5°) for all Mnk systems,

Table 6. Average Distances between Selected Heavy Atoms Close to the Metal Binding Site for All Apo Forms of Menkes MBDs and from the Last 15 ns of 30 ns MD Runs (session 2)[a]

	Mnk1	Mnk2	Mnk3	Mnk4	Mnk5	Mnk6
T13(Oγ)−Cys1(S)	4.6 (0.8)	4.2 (0.7)	9.0 (0.6)	7.5 (0.8)	5.6 (1.3)	5.5 (1.5)
Cys1(S)−S16(Oγ)	5.0 (1.1)	4.4 (0.9)	9.2 (0.7)	8.5 (1.0)	6.5 (1.9)	5.6 (1.7)
S16(Oγ)−Cys2(S)	6.2 (1.5)	5.3 (1.0)	6.3 (0.5)	6.9 (1.5)	7.0 (0.9)	5.3 (1.1)
Cys2(S)−F66(Cζ)	6.1 (1.5)	4.2 (0.5)	3.9 (0.5)	3.8 (0.3)	5.0 (1.0)	4.6 (0.7)
Cys1(S)−Cys2(S)	5.0 (1.1)	4.8 (1.0)	6.9 (0.6)	8.4 (0.7)	5.9 (1.0)	6.1 (1.6)

[a] rmsds are given in parentheses. Subtract 1 from all residue numbers for Mnk6.

dx.doi.org/10.1021/bi300669e | *Biochemistry* 2012, 51, 8885−8906

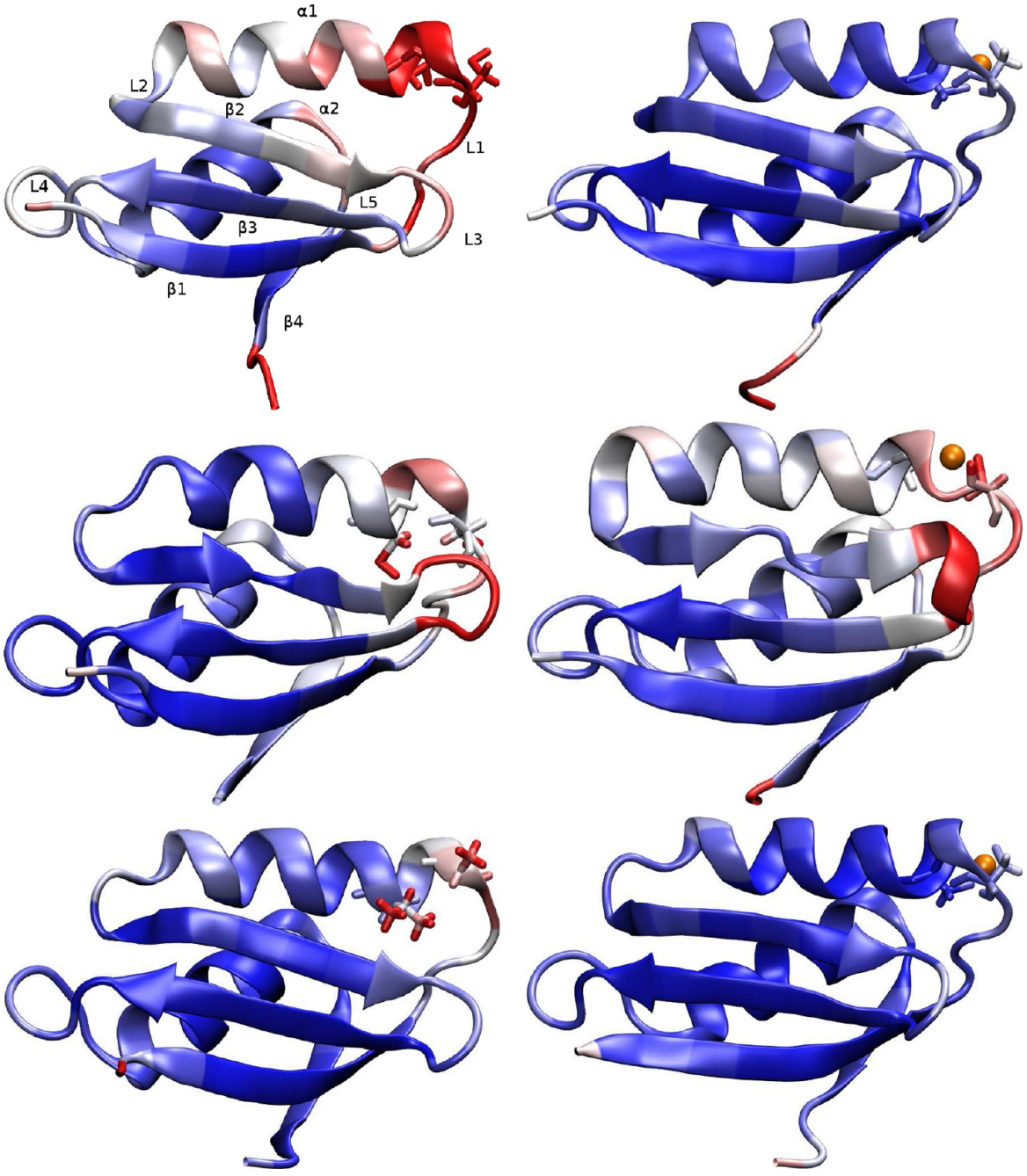

Figure 7. Average structures of Mnk1, Mnk5, and Mnk6, in their apo (left) and holo (right) forms, calculated over the last 15 ns of the 30 ns MD runs (session 2). Mnk1−6 from top to bottom and from left to right. Only secondary structure elements, the two cysteine residues, and the Cu^{I} ion forming the MBS are represented. The structures were averaged over 15 ns MD and then energy-minimized (see Details of the MD Simulation), and all atom rmsds from the initial NMR structure were calculated. Atoms are then color coded from blue to red corresponding to these backbone atom coordinate rmsds from 0.5 to 1.5 Å, respectively. This figure was drawn with VMD.[44]

meaning that there is a significant departure from linearity of the S−Cu^{I}−S angle (the equilibrium angle being 180°). The distances between T13(Oγ) and Cu^{I} (5.0 Å), S16(Oγ) and Cu^{I} (5.0 Å), and Cys1(O) and Cu^{I} (3.5 Å) are identical for Mnk1, Mnk2, Mnk4, and Mnk6. Cys1(N) and Cys2(N) with distances from Cu^{I} equal to 2.8 and 3.0 Å, respectively, act as potential secondary ligands. The average S16(Oγ)−Cu^{I} (5.4 Å) and Cys1(O)−Cu^{I} (4.4 Å) distances increase and present larger fluctuations in the case of Mnk5. Noticeably, the interaction between the hydroxyl oxygen of Thr13 and copper is lost in Mnk5 (distance of 7.0 Å) (and of course in Mnk3 where this residue is changed to His).

The distances between other atoms of the MBS susceptible to coordination of the metal have been analyzed. In general for Mnk1, Mnk4, and Mnk6, most of the average distances between heavy atoms selected in Table 6 become shorter with smaller fluctuations. As an example, for Mnk1 holo, we measure (from our energy-minimized MD averaged structure) a T13(Oγ)−Cys1(S) distance of 4.4 Å, a Cys1(S)−S16(Oγ) distance of 3.8 Å, and a Cys2(S)−F66(Cζ) distance of 4.5 Å.

dx.doi.org/10.1021/bi300669e | *Biochemistry* 2012, 51, 8885−8906

Average Structures. Finally, to illustrate the previous results, energy-minimized average structures of Mnk1, Mnk5, and Mnk6 calculated over the last 15 ns of the 30 ns MD runs are shown in Figure 7. The figure nicely summarizes and completes results obtained from the analysis of rmsfs. Globally, Mnk6 [and also Mnk2−4 (not shown)] appear more stable than Mnk1 and -5; in more detail, we observe large to moderate fluctuations of loops L1 and L3 and the beginning of helix α1 for Mnk1, -5, and -6 in their apo forms; strong stabilization of L1 and α1 in Mnk1 and -6 but even greater fluctuations in Mnk5 upon Cu^I binding; large fluctuations of loops L1 (including metal bound cysteines) and L3 and the beginning of helices α1 and α2 for Mnk5 holo; and moderate fluctuations in general at the N- and C-termini except for Mnk1, which shows very large fluctuations of its C-terminus.

More specifically, an analysis with Stride of helix α1 in the energy-minimized MD averaged structure of Mnk3 shows that this helix numbers 14 amino acids in the apo form, C14−A27, and is reduced to 13 amino acids after metal binding. This observation results from the absence of an H-bond between C14(O) and V18(H) in the NMR structure of the holo form,[26] which translates into one fewer restraint in our simulations and an average distance between C14(O) and V18(H) that increases from 2.0 to 2.8 Å.

In the case of Mnk5 holo, I34 and L35 act as strand breakers preceding the highly fluctuating loop L3, which forms a 3−10-helix from L38 to A40.

After studying the dynamics of HAH1[18] and, in this work, the dynamics and stability of all metal binding domains of its partner ATPase, we now address the issue of the interactions between the two partners. Are they governed mainly by electrostatics, which has been a question of debate,[45] and which one of the sixMBDs is predicted to interact more favorably with the chaperone given its structure as an isolated entity?

Electrostatic Interactions between HAH1 and Menkes MBDs. *Interactions of Dipole-Oriented Partners.* In the process of conveying Cu^I to the ATPase, HAH1 is globally neutral (zero total charge) but HAH1 bears a strong dipole moment between two opposite faces. Its positive face due to the presence of one Arg and Lys in helix α1 and three Lys residues in helix α2[17] interacts with the negatively charged face of Mnk1 in the resolved Mnk1−HAH1 complex[19] (PDB entry 2K1R).

Dipole moments of HAH1 and the six MBDs were calculated with CHARMM in both their apo and holo form and are summarized in Table 7. Coordinates used for the calculations were taken from the NMR structures. The calculations of the dipole moments were conducted with the all-atom CHARMM27 force field for better precision. The last column of the table gives the values obtained with the CHARMM19 force field that was used in the docking simulations and shows that they are close to the more accurate CHARMM27 results (Cu^I form of HAH1 and apo form of the Menkes MBDs). All apo MBDs except Mnk2 bear a negative or zero total charge. Mnk1 and Mnk4 (apo) have a large total charge of −5 and large dipole moments. Mnk5 also bears a relatively large dipole moment compared to Mnk2 or Mnk6.

Starting from the oriented dipole configuration (see Docking with CHARMM), we find the dipole−dipole interaction energies between HAH1 and MBDs are all attractive. At long distances, the charge repulsion energy will dominate the total interaction for Mnk1 and Mnk4.

Table 7. Comparison of the Charge (q) and Module of the Electric Dipole Moment (μ) for Metallochaperone HAH1 and the Six Menkes Metal Binding Domains[a]

	holo (Cu^I)		apo		HAH1 (Cu^I)−Mnk (apo)
	q (C)	μ (D), CHARMM27	q (C)	μ (D), CHARMM27	μ (D), CHARMM19
HAH1	−1	271	0	318	278
Mnk1	−6	251	−5	271	264
Mnk2	1	104	2	156	161
Mnk3	−2	190	−1	168	172
Mnk4	−6	285	−5	260	250
Mnk5	−1	229	0	240	236
Mnk6	−1	95	0	168	157

[a]Calculations were done using the CHARMM27 (all atom) force field for columns 3 and 5 and using the CHARMM19 (extended carbon) force field for column 6 (Cu^I form of HAH1 and apo form of the Menkes MBDs in that column). HAH1 was capped using the standard NTER (NH_3^+) and CTER (COO^-) termini, whereas the MBDs were capped with the neutral ACE (CH_3) and CT2 (NH_2) termini in the CHARMM27 calculation and left uncapped in the CHARMM19 calculation.

Then, the partners were rotated by 90° around the Y axis to show their interacting surface (assuming that this interaction is driven by electrostatics) and are shown in Figure 8.

Mnk1 and Mnk4 share the same orientation of their secondary structure elements when their dipoles are aligned so that they best interact with HAH1. Mnk2 and Mnk5 seem to be rotated around the Y axis, and Mnk3 and Mnk6 have a completely different orientation.

Docking Simulations of HAH1 on Menkes MBDs. *Results of Docking with CHARMM.* After translating HAH1 toward each Mnk MBD until the interaction energy between HAH1 and Mnk became positive (see Docking with CHARMM, stage 1), we listed the properties of the structures with minimal interaction energy along the path in Table 8

Mnk1 and Mnk2 show a proper orientation of their MBS cysteines with a short Cu^I−S distance at the lowest interaction energy point along the path, but the Mnk2 dipole and the interaction energy with HAH1 are the smallest of those of all MBDs. As already noticed, the electrostatic dipole is larger for Mnk1, Mnk4, and Mnk5 than for the other MBDs, but the lowest interaction energy corresponding to a high dipole, as well, is seen in the case of Mnk3. The observation of the structure shows that this is due to the proximity of D2 in Mnk3 to K56 and K57 in HAH1, while the large interaction energy between Mnk6 and HAH1 comes from the direct electrostatic interaction between D49 in Mnk6 and K56 in HAH1. A large interaction energy is also observed between E55 in Mnk4 and the latter lysine residue in HAH1. Starting from the coordinates of the partners in the NMR complex (Mnk1HAH1), we obtained a large interaction energy as well because of electrostatic interactions between D67 in Mnk1 and both K25 and K57 in HAH1 and between E10 in Mnk1 and K25 in HAH1. Notice that interprotein contacts with D67 in Mnk1 and K57 in HAH1 were also observed in the structure of the complex but not with K25 in HAH1 or E10 in Mnk1.

In the following stage of the docking with CHARMM, copper was removed and a distance restraint on δSS was applied to force a contact between the two partners mediated by dipolar interaction. After the 1 ns restrained dynamics forcing the cysteines of the MBS to come in contact for

dx.doi.org/10.1021/bi300669e | Biochemistry 2012, 51, 8885−8906

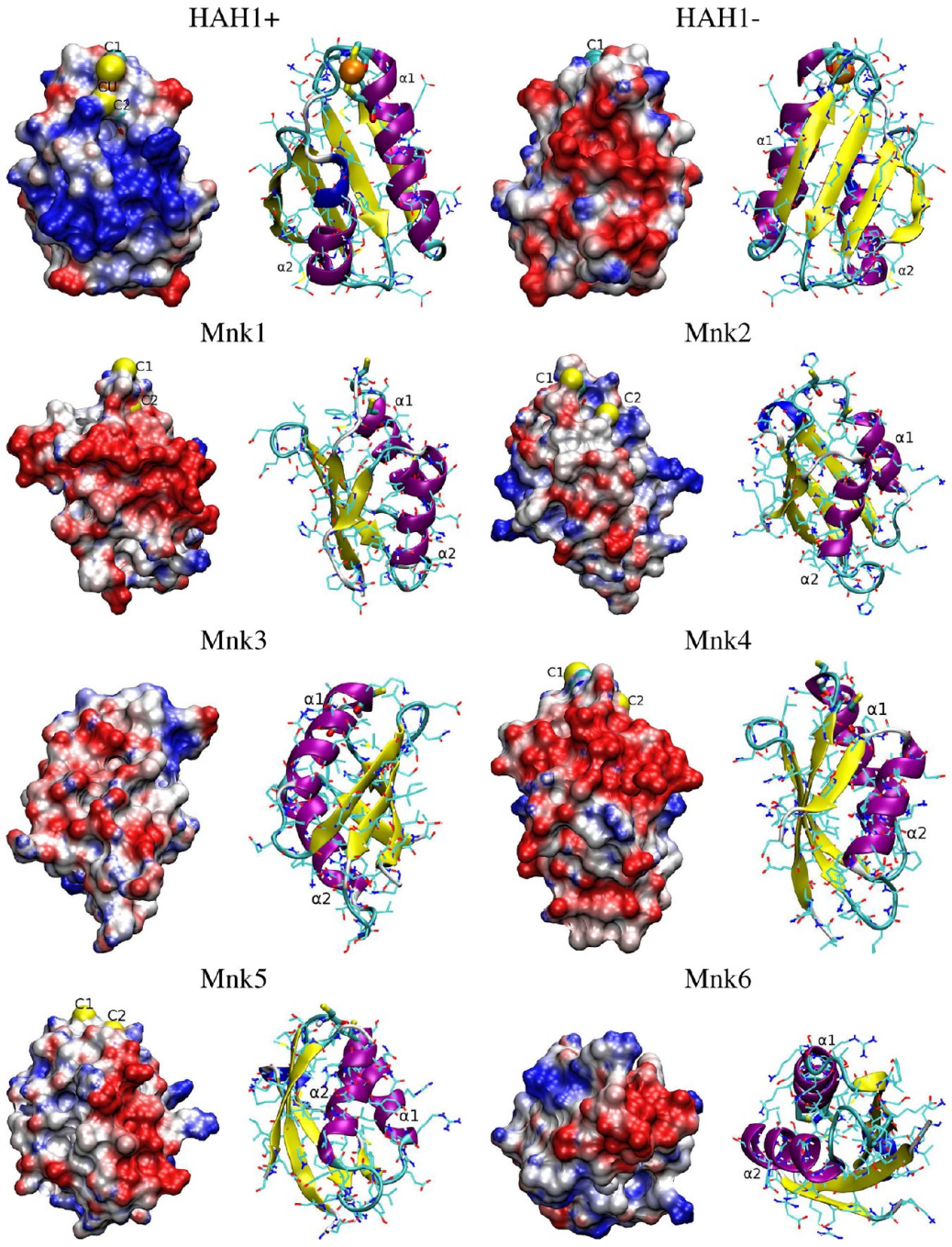

Figure 8. Electrostatic potential maps and corresponding secondary structures for all apo Menkes MBDs and holo metallochaperone HAH1. MBDs are oriented to show the "face" corresponding to the most negative potential, whereas both most positive (+) and most negative (−) potential faces are shown for HAH1 (first line). The metal binding cysteines are drawn in CPK representation with outstanding yellow spheres corresponding to sulfur atoms and labeled Cys1 and Cys2 for the first and second cysteines in the sequence, respectively. The metal bound to HAH1 is represented by an orange van der Waals sphere. Helices $\alpha 1$ and $\alpha 2$ are labeled in the secondary structure representations. The structures were drawn with VMD,[44] and electrostatic maps were calculated with Adaptive Poisson−Boltzmann Solver (APBS)[46] within VMD.

potential copper exchange and energy minimization (see Docking with CHARMM, stage 2), interaction energies between HAH1 and each MBD together with δSS are reported in Table 9. The values from the last MD simulation after release of the restraints on δSS (stage 3) are also given in parentheses.

van der Waals (vdW) interaction energies between HAH1 and the MBDs are similar for all MBDs and 3−5 times smaller than electrostatic interaction energies. Mnk1, Mnk3, Mnk4, and Mnk6 show the largest interaction energies between the partners with a maximum for Mnk4. The energies corresponding to the simulations run from the coordinates of Mnk1 and HAH1 as found in the NMR structure of the complex (Mnk1HAH1 row) are comparable to their counterparts obtained from the coordinates of the isolated proteins (Mnk1 row). Not surprisingly, release of the restraints on the distance between the cysteines of the MBS results in an average increase in this distance. The largest increase is observed for Mnk4−6 and is accompanied by a large increase in the electrostatic interaction energy. This probably means that electrostatics drives these proteins away from a structure where metal transfer

dx.doi.org/10.1021/bi300669e | *Biochemistry* 2012, 51, 8885−8906

Table 8[a]

	Mnk1	Mnk2	Mnk3	Mnk4	Mnk5	Mnk6	Mnk1HAH1
int. *E* (kcal/mol)	−104	−29	−198	−160	−65	−134	−176
Cu^{I}–S distance (Å)	13.5	11.6	28.9	17.9	20.1	38.0	15.2
Mnk dipole (D)	210	117	194	239	199	183	191

[a]HAH1 was slowly translated toward Mnk. The minimal CHARMM interaction energy between the two proteins along the path is given as int. *E*. The corresponding distance between Cu^{I} (bound to HAH1) and the midpoint between the two S atoms of the metal binding cysteines and the electrostatic dipole of the MBD are also given. The Mnk1HAH1 column stands for a docking simulation starting from the structure of HAH1 and Mnk1 found in the NMR complex[19] (PDB entry 2K1R).

Table 9. CHARMM Interaction Energies after 1 ns Dynamics and Minimization (stage 2 with the CHARMM19 extended atom force field using a nonbonded cutoff of 13 Å and atom FSHIFT, VSHIFT cutoff schemes)[a]

	vdW (kcal/mol)	electric (kcal/mol)	total (kcal/mol)	δSS (Å)
Mnk1	−69 (−71)	−296 (−338)	−365 (−409)	4.6 (9.4)
Mnk2	−55 (−48)	−158 (−151)	−214 (−199)	4.2 (4.5)
Mnk3	−83 (−84)	−325 (−375)	−407 (−459)	4.9 (6.0)
Mnk4	−88 (−88)	−377 (−478)	−465 (−566)	5.5 (9.9)
Mnk5	−83 (−84)	−253 (−297)	−337 (−381)	4.5 (7.7)
Mnk6	−75 (−81)	−352 (−481)	−426 (−562)	5.6 (12.2)
Mnk1HAH1	−57 (−50)	−287 (−386)	−344 (−436)	4.7 (7.0)

[a]Distance δSS reported in column 5. The results of the configurations obtained after a 1 ns supplementary MD run with no restraint on δSS (stage 3) are given in parentheses. The Mnk1HAH1 row represents the simulations started from the coordinates of Mnk1 and HAH1 as found in the NMR structure of the complex.

Table 10. Interaction Energies, Distances between Metal Binding Cysteines, and rmsds from the NMR-Determined Structure of the Complex between HAH1 and Mnk1 (PDB entry 2K1R) from Dockings Obtained with Seven Docking Programs with CHARMM[a]

	complex			isolated		
program	interaction *E* (kcal/mol)	δSS (Å)	rmsd (Å)	interaction *E* (kcal/mol)	δSS (Å)	rmsd (Å)
HEX	−180.4	14.9	13.5 (29.6)	−191.3	26.5	13.9 (23.0)
Haddock	−393.2	10.1	2.1 (4.3)	−395.6	7.8	4.1 (7.9)
ClusPro	−318.5	4.3	2.6 (5.6)	−418.7	7.7	3.9 (7.7)
ATTRACT	−126.5	27.3	13.5 (34.3)	−232.9	23.5	12.8 (26.3)
ZDock	−363.3	3.3	2.5 (3.8)	−301.4	6.1	3.5 (6.6)
PatchDock	−84.5	14.6	15.1 (29.7)	−142.1	20.9	9.3 (20.6)
GRAMM-X	−286.9	4.4	0.7 (1.1)	−18.8	8.3	8.6 (24.2)
CHARMM	−349.0	4.7	6.4 (12.1)	−362.9	4.8	6.8 (8.8)

[a]Parameters and models kept for the different programs are described in Docking with Several Docking Programs, and for CHARMM, structures obtained after stage 2 were used (see Docking with CHARMM). Energies were evaluated with the CHARMM19 extended atom force field using a nonbonded cutoff of 13 Å and the atom FSWITCH, VSHIFT cutoff schemes. Harmonic restraints on all non-hydrogen atoms (force constant of 5 kcal mol^{-1} $Å^{-2}$) were introduced to keep the minimized structure close to the output of the docking. Interaction energies, δSS values, and atomic rmsds from the energy-minimized experimental structure of the complex are reported after an ABNR energy minimization down to a gradient of 0.01 kcal mol^{-1} $Å^{-1}$. rmsds are calculated for the whole complex after superimposition of all non-hydrogen atoms or, in parentheses, of HAH1 backbone atoms, only.

would be possible. This overly large value of δSS is observed for all MBDs except Mnk2 (and possibly Mnk3). There may be several reasons explaining the low probability of finding the structure of the complex with CHARMM. (i) Simulations are run in vacuum with a dielectric constant ε of 1 that will overestimate the contribution of electrostatic energies to the total interaction energy between the partners. We did try a slightly better model, though, with the same simulations in an implicit solvent with the EEF1 potential (effective energy function 1),[47] but with no real improvement. (ii) Large rearrangements of the side chains of some interacting residues not accessible with such short and "crude" simulations may be necessary to reach the structure of the complex. (iii) Finally, the hypothesis that the two partners come into contact with aligned electric dipoles maximizing their electrostatic interaction at long distances may be too restrictive. Stuck into an electrostatic minimum, the two partners would probably not be able to reorient properly to form the natural complex in 1 ns. The simulations started from the structures found in the NMR complex are instructive: the partners show similar electrostatic interaction energies as they do starting from the isolated structures, but release of the restraints on δSS increases this distance by only 2.3 Å instead of 4.8 Å in row 1. The final distance, 7.0 Å, is still a bit long to allow copper exchange.

Docking with Several Docking Programs. Other than CHARMM MDs, several docking experiments were run starting from the oriented dipole configurations. Seven standard protein–protein docking programs were used to see how rigid body docking could explain the interactions between the metallochaperone and MBDs of the ATPase.

The docking programs were tested by comparing their performances on the known structure of the complex between

Table 11. Results of the Best Docking Scores of HAH1 on Menkes MBDs for All the Programs Tested (except GRAMM-X, which does not report any score, and CHARMM, for which a score could be defined as the interaction energy given in Table 12)[a]

protein	HEX energy	Haddock energy	ClusPro energy	ATTRACT energy	ZDock score	PatchDock score
Mnk1	−467.3	−324.4	−563.3	−29.3	696.924	5134
Mnk2	–	−177.2	−451.5	−31.4	681.023	6086
Mnk3	−435.4	−162.0	−490.6	−31.5	482.279	4200
Mnk4	−452.3	−270.2	−521.9	−30.5	616.357	5252
Mnk5	−420.9	−241.3	−518.4	−32.0	–	4790
Mnk6	−456.6	−143.9	−487.6	−29.7	558.363	6194
Mnk1HAH1	−413.5	−339.9	−691.3	−30.0	849.415	6622

[a]Parameters and models kept for the different programs are described in Docking with Several Docking Programs (HEX was not able to predict a model of the Mnk2 complex, and ZDock was not able to predict a model of the complex of Mnk5 with HAH1). The Mnk1HAH1 row represents the dockings started from the coordinates of Mnk1 and HAH1 as found in the NMR structure of the complex.

Table 12. Interaction Energies between HAH1 and All Menkes MBDs after Docking with Four Standard Docking Programs (with CHARMM) and Energy Minimization with CHARMM[a]

	Haddock		ClusPro		ZDock		GRAMM-X		CHARMM	
MBD	interaction *E*	δSS	interaction *E*	δSS	interaction *E*	δSS	interaction *E*	δSS	interaction *E*	δSS
Mnk1	−378.2	7.8	−405.5	7.7	−252.5	6.0	−0.3	8.3	−409.1	9.4
Mnk2	−123.1	3.2	−243.2	31.9	−55.7	5.3	−59.6	9.2	−199.2	4.5
Mnk3	−93.3	8.7	−262.1	15.2	−103.9	13.1	−59.4	12.4	−459.2	6.0
Mnk4	−270.1	7.3	−289.5	5.4	−260.9	7.8	−272.9	3.8	−565.6	9.9
Mnk5	−212.2	6.5	−236.1	36.1	–	–	−88.9	3.3	−381.1	7.7
Mnk6	−80.7	8.1	−376.2	25.0	−137.9	17.2	−81.8	9.8	−561.9	12.2

[a]The δSS distances between sulfur atoms of the MBS cysteines are also given. As previously, parameters and models kept for the different programs are described in Docking with Several Docking Programs, and for CHARMM, structures obtained after stage 3 and energy minimization (with the FSWITCH, VSHIFT cutoff scheme), in the absence of distance restraints maintaining the secondary structures, were used (see Docking with CHARMM).

HAH1 and Mnk1 from NMR experiments[19] (PDB entry 2K1R). The programs were given as input the separated structures of the two partners coming from either the structure of the complex itself or the structures of the isolated proteins (see Table 1) to test the influence of small structural changes (induced fit) in the two proteins caused by the formation of the complex. The results of interaction energies between partners (as calculated with the CHARMM19 force field), δSS, and rmsd from the NMR structure of PDB entry 2K1R are listed in Table 10. CHARMM docked structures after stage 2 (with restraints on δSS) were used for the CHARMM row of this table and subjected to the same minimizations that were described for the other programs in the legend. The values obtained directly from the NMR structure of the complex after similar minimization with harmonic restraints are as follows: interaction *E* = −287.4 kcal/mol, δSS = 4.8 Å, and rmsd = 0.1 Å. Thus, CHARMM docked structures give interaction energies on the order of −350 kcal/mol (very close, fortunately, to those obtained with the different cutoff scheme in Table 9), significantly larger than the interaction energy measured from the NMR structure of the complex with similar δSS values (due to the restraints) and large rmsds (≥6 kcal/mol) away from that structure. As mentioned earlier, this probably means that a better CHARMM docking protocol might be obtained by lowering the contribution of the electrostatic energy to the total energy of the complex. The result obtained with model 1 of GRAMM-X is obviously wrong because of the very small interaction energy; indeed, using model 2, a much better fit to the NMR complex is obtained: interaction *E* = −211.0 kcal/mol, δSS = 7.2 Å, and rmsd = 5.9 Å [note, again, that because the structure of the complex between HAH1 and Mnk1 (PDB entry 2K1R) is known from M5 to N73 and the structure of the isolated Mnk1 (PDB entry 1KVI) from G6 to D79, common residues G6−N73 were used here].

The lowest rmsds starting from separated structures of the partners in the complex were obtained with GRAMM-X, Haddock, ZDock, and ClusPro, in this order. Starting from structures of the isolated partners, Haddock, ZDock, and ClusPro still do a good job. These programs are also those that give the smallest values of the distance between MBS cysteines (δSS). HEX, ATTRACT, and PatchDock give very bad results, with the coordinate rmsd from the NMR structure ranging from 13.5 to 15.1 Å.

Then these programs were used to predict the structures of the unknown complexes between HAH1 and all MBDs using the same parameters that were used previously. The energies or scores of all the programs are listed in Table 11.

The complex with Mnk1 realizes its best docking score with HEX and Haddock. Interestingly, the complex obtained from the structure of PDB entry 2K1R gives outstandingly good scores with ClusPro, ZDock, and PatchDock, although we have seen that, for the latter, δSS and rmsd from PDB entry 2K1R are unacceptably high. Docking of HAH1 on Mnk3 produces low scores with most programs, especially with Haddock, ZDock, and PatchDock. Notice that the Haddock scores listed here are much higher than those reported in Table 3 of Banci et al.[19] This is due to the fact that they defined active and passive residues from the information obtained from the NMR complex between Mnk1 and HAH1, whereas we were much less restrictive by defining only the four amino acids, including the metal binding cysteines (CxxC) of each protein, as being active. Nevertheless, we obtain almost the same Haddock

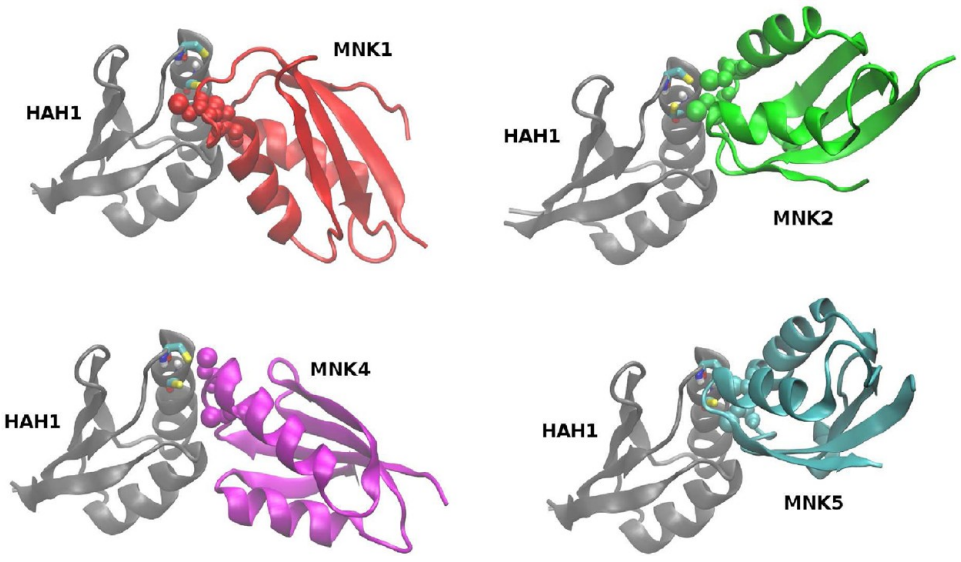

Figure 9. Models of the complexes between HAH1 and four of six Menkes metal binding domains obtained using several docking programs. These structures correspond to the shortest δSS distance between sulfur atoms of the MBS cysteines obtained with these programs. Complexes are ranked HAH1 vs Mnk1 and Mnk2 (top row) and Mnk4 and Mnk5 (bottom row), from left to right, respectively, and seen in the same orientation as the NMR complex (PDB entry 2K1R) in Figure 1 of ref 19. Secondary structures are shown, and the cysteines of the MBS are represented in licorice and vdW modes for HAH1 and the MBDs, respectively.

Table 13. Interface Areas and Interface Residues between the Menkes MBDs and HAH1 from the Complexes Proposed Here[a]

MBD	interface area (Å^2)	HAH1 interface residues	Mnk interface residues
Mnk1	666	D9, T11, C12, C15, A18, R21, V22, K25, K57, T58, G59, K60, T61	M12, T13, C14, S16, C17, T20, I61, D62, D63, M64, G65, F66, D67, A68
Mnk2	398	C12, G14, C15, E17, R21, T58, K60	G11, M12, T13, C14, H15, S16, C17, D39
Mnk4	497	C12, C15, A18, R21, V22, K25, K56, K57, T58, G59, K60	I9, D10, G11, M12, T13, C14, S16, C17, L38, S41, G65, F66, D67
Mnk5	489	T11, C12, G14, C15, E17, A18, R21, K57, T58, G59, K60	T10, G11, T13, C14, A15, S16, C17, N20, L38, L64, F66
Mnk1HAH1	590	T11, C12, G14, C15, R21, V22, K25, K57, T58, G59, K60	C14, N15, S16, C17, T20, Q24, D62, D63, G65, F66, D67

[a]The last row corresponds to the same analysis run on the NMR resolved complex between Mnk1 and HAH1. The interface area is calculated as half the difference between the sum of contact surfaces between the two separated partners and the contact surface of the partners in the complex. Interface residues are defined as residues with at least one atom that is <3.5 Å from any atom in the other protein.

scoring order: Mnk1HAH1 > Mnk1 > Mnk4 > Mnk5 > Mnk2 > Mnk3 > Mnk6.

To quantitatively compare the structures obtained after docking with the different programs, the interaction energies between partners and δSS distances between cysteines of the MBS were all calculated with CHARMM following the same protocol. All structures were read and corrected for residue numbering or atom names to comply with the CHARMM nomenclature. The CHARMM19 force field was used for calculating energies in vacuum using a nonbonded cutoff of 13 Å and the recommended atom FSWITCH, VSHIFT cutoff schemes (more precise than the FSHIFT option used above). Harmonic restraints were set on all non-hydrogen atoms with a force constant of 5 kcal mol^{-1} Å^{-2}, and the structures of the complexes were energy-minimized down to a gradient of 0.01 kcal mol^{-1} Å^{-1}. Interaction energies between partners and measured values of δSS are reported in Table 12. CHARMM docked structures after stage 3 (after releasing the restraints on δSS) were used for the CHARMM column of this table.

With δSS values of >6.0 Å with all programs, results of the dockings are not convincing for Mnk3 and Mnk6. For the other MBDs, on the other hand, there is a relatively good consensus between the results of the different docking programs. The complex with Mnk4 is favored with CHARMM. The structures of the complexes giving the lowest δSS values and thus compatible with copper exchange between the partners were selected in the following discussion and for visualization: Mnk1 from ZDOCK, Mnk2 from Haddock, and Mnk4 and Mnk5 from GRAMM-X. Corresponding CHARMM interaction energies with HAH1 are −252.5, −123.1, −272.9, and −88.9 kcal/mol, respectively. Banci et al. observed that the copper transfer properties between HAH1 and Mnk2 or Mnk5 are similar,[16] and they did not detect an adduct between Mnk2/Mnk5 and HAH1, suggesting weak interactions between the partners. Our results are in good agreement with this observation: the interaction energies between HAH1 and Mnk2 or Mnk5 in Table 12 are low relative to those of the other Mnks; they are even lowest for ClusPro, ZDock, and CHARMM.

Then the backbone atoms of HAH1 in each selected structure were superimposed with the corresponding atoms in the NMR complex (PDB entry 2K1R), and the docked partners are shown in Figure 9.

The top left structure corresponds to the docking of "isolated" proteins HAH1 and Mnk1 following the nomenclature given in the results of Table 10. The structure of the complex is rather close to the NMR structure (3.5 Å rmsd), and it is also the structure with the best ZDOCK score (see Table

dx.doi.org/10.1021/bi300669e | Biochemistry 2012, 51, 8885−8906

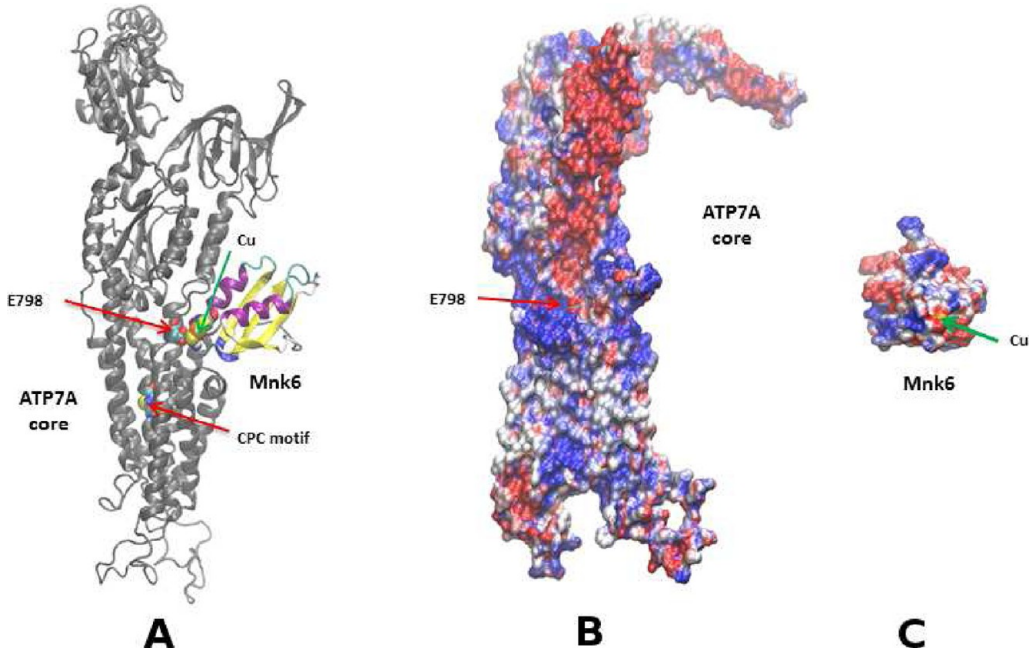

Figure 10. (A) Docking of Mnk6 on the ATP7A core (Haddock model). (B) Electrostatic potential map of the ATP7A core in the interface region with Mnk6 after rotating panel A by 90° anticlockwise around the membrane normal. (C) Electrostatic potential map of Mnk6 in the interface region with the ATP7A core after rotating panel A by 90° clockwise. By convention, blue and red colors represent positive and negative potentials, respectively.

11). Our model of the docking of Mnk4 suggests that its interface with HAH1 implies amino acids common to Mnk1. The best docking of Mnk4 is obtained with GRAMM-X with an outstandingly high measured CHARMM interaction energy between the partners (see Table 12). Our models of the complexes with Mnk2 and Mnk5 also seem to share a similar interface with HAH1. These last points appear clearly from Table 13, where we have listed the interface areas and interface residues between the two partners. Interface residues will consist of MBS cysteines and surroundings due to the way we selected the best models. Interface residues in HAH1 include C12, C15, R21, T58, and K60 in all complexes, whereas a common motif between MBDs consists of MBS residues C14, S16, and C17. Interface residues between HAH1 and Mnk1 in the NMR complex (Mnk1HAH1 row) are logically the same as those reported by Banci et al.[19] (although the method for defining them is probably different). They are also almost the same as those obtained from the two separated proteins (Mnk1 row), which makes our docking approach more credible. We can notice the implication of the hydrophobic stabilizing residue F66 at the interface and again the same behavior of Mnk1 and Mnk4 with a large interface area and many common residues at this interface like T13, G65, and D67.

Finally, we predicted a possible docking interface between Mnk6 and ATP7A. The initial coordinates of the ATP7A protein were taken from the recent modeling by Gourdon et al.[20] and downloaded from the *pumpkin* Web site (http://www.pumpkin.au.dk/atp7ab/). We used our experience on the docking of Mnk systems to choose the best docking program for the interaction between Mnk6 and the ATP7A protein core. Among ClusPro, GrammX, ZDock, and Haddock, only Haddock gave reproducible results compatible with the presence of a membrane surrounding a large part of ATP7A (docking simulations are run in vacuum, and the three other programs proposed docking positions for Mnk6 below the membrane plane). In the following, we briefly analyze the structure proposed by Gourdon et al. for the Mnk6−ATP7A interface (GourdMod model) and propose another interaction model based on the docking simulation with Haddock (Haddock model). For the GourdMod model, coordinates of ATP7A and Mnk6 from E561 to P1413 were extracted from file *ATP7A_With_HMBDs_02.pdb* on the *pumpkin* server and coordinates for missing residues A638−H640 built from internal coordinates with CHARMM. For our Haddock model, coordinates of the ATP7A protein core from L641 to P1413 were taken from file *ATP7A_Without_HMBDs_02.pdb* on the server and coordinates of Mnk6 from the NMR structure of this MBD (PDB entry 1YJU) as in the rest of this work.

For this last docking, we have assumed, following an idea of Gourdon et al., that the entry point for copper could be E798 (equivalent to E205 in the structure of LpCopA),[9] and we have introduced distance restraints accordingly in the docking program between the E798 Oε atom and C575 and C578 S atoms. The resulting model yields a very good score of −528 kcal/mol (see Table 15) with good reliability (112 models in the cluster of 200 models). We then introduced Cu^{I} in the two models (GourdMod and Haddock) approximately between the sulfur atoms of the two charged MBS cysteines and minimized the energy of the models with CHARMM (CHARMM19 force field and our force field for copper) with harmonic restraints on backbone atoms down to a gradient of 0.01 kcal mol^{-1} $Å^{-1}$. The Haddock model structure of the E561−P1413 part of the Menkes ATPase is shown in Figure 10. Mnk6 appears to be correctly positioned for the transfer of copper to E798 (for instance), and its N-terminal part protrudes into the solvent largely above the membrane plane, which is compatible with its binding to Mnk5 and the N-terminal part of ATP7A.

Clearly, the short distance of 6.8 Å obtained in our model from the copper ion to the E798 Oε atoms suggests that this

Table 14. Interface Residues (polar only) between Mnk6 and the ATPase Core for the Two Models Studied[a]

model	Mnk6 interface residues	ATP7A interface residues
GourdMod	D1, E49, K71, K72, D73	D642, K644, R648, R651, K811
Haddock	M11, T12, S15, H18, K19, E21, S22, S23, K26, R28, Y32, C33, S34, N40, H43, E66, K72	D642, H643, R645, E646, Q734, K737, K742, N745, D747, R795, E798, H799, K802, T805, S806, E840, E921, E922, Q924, T925, S926

[a]Again, interface residues are defined as residues with at least one atom that is <3.5 Å from any atom in the other protein. The numbering for Mnk6 refers to the isolated sequence studied in this work; add 562 to reach the sequence number in the whole ATP7A protein.

idea of direct transfer of Cu^I to the translocation pathway in ATP7A may indeed be possible.

Hydrogen bonds between interface residues have been analyzed (distance between acceptor and donor of <2.4 Å and maximal out of line donor−hydrogen−acceptor angle of 120°). In the GourdMod model, D1 and E49 interact with K811, K72 interacts with D642, and D73 interacts with R651. In our model, many more hydrogen bonds between Mnk6 and the protein core are found, namely, between T12 and Q734, S15 and E798, E21 and R645, S22 and E921, K26 and E922, R28 and E840, Y32 and D642, S34 and R645, N40 and K737, E66 and K742, and finally K72 and D642.

The resulting interaction energy between Mnk6 and the ATP7A core, the interface area, and the distance between Cu^I and E798 are listed in Table 15 and clearly discriminate between the two models. Our model is compatible with a direct transfer of Cu^I from Mnk6 to the ATP7A core, and Gourdon's model is not.

Table 15. Analyses of ATP7A Model Structures from E561 to P1413, Including the Last MBD (Mnk6) from E561 to D635[a]

model	interaction energy (kcal/mol)	interface area (Å^2)	Cu^I−E798 Oε distance (Å)
GourdMod	−282.7	326	42.9
Haddock	−589.6	1386	6.8

[a]GourdMod is a model by Gourdon et al. extracted from the *pumpkin* server, and Haddock is our docking model of Mnk6 on the ATPase core (see the text). Both models were energy-minimized using the CHARMM19 force field prior to the calculation of interaction energies and interface areas (see Table 13) between Mnk6 and the protein core. The average distance between the two Oε atoms of E798 and copper is given in the last column.

DISCUSSION AND CONCLUSION

It has been proposed that the homeostasis of copper in cells is the result of the contribution of several pathways involving weak protein−protein interactions.[19] In humans, the Menkes and Wilson proteins possess a long N-terminal tail containing six Cu^I binding domains. Copper is exchanged from metallochaperone HAH1 to one or several MBDs of the ATPases.[48] Surface plasmon resonance experiments have shown that all the metal binding sites of the Menkes protein were involved in binding of copper-loaded HAH1 and that the interaction between the two partners was transient, was of a non-cooperative nature, and indicated similar binding constants on the order of 10^5−10^6 M,[49] but after experimenting and modeling for several years, the precise role of each MBD remains unclear and the structure of the bundle of six MBDs is unknown.

To clarify these ideas from a dynamical and electrostatic point of view, we have carefully simulated and analyzed the dynamics of the six MBDs of the Menkes protein starting from the coordinates of their solution structure. All the simulations were run on isolated MBDs, whereas they are probably tightly packed in the real protein. Some of them were unstable during the simulations, showing large coordinate rmsds from the initial structure (session 1); we corrected this problem by introducing distance restraints maintaining the secondary structure elements of the proteins through their H-bonds (session 2). It has been known for a long time that hydrogen bonding stabilizes globular proteins,[50] and introducing restraints that would maintain H-bonds in MBDs seemed natural. Quite common, as well, is the introduction of restraints into the molecular system on heavy atoms far from a particular region of interest to avoid deviations from the experimentally determined structure (see, for instance, ref 51 for a recent example). The reasons why some of our simulations of MBDs were unstable may have several possible causes. (i) The systems may have been improperly equilibrated without restraints, and releasing them after, say, 20 ns in session 2 might have resulted in stable structures in longer dynamics in the absence of restraints. (ii) Study of the alanine dipeptide energy map showed important discrepancies between the CHARMM27 force field and DFT calculations,[51] but this problem was solved in 2004 with the publication of the CMAP correction[52] that we have used in this work. (iii) The highly conserved residue F66 in the MBDs presents an aromatic side chain facing the metal binding loop that contributes importantly to the stability of a substantial portion of the protein structure.[24] In proteins, the rings of phenylalanine residues typically interact with other residues via the T-shape or parallel-displaced conformations. The CHARMM potential energy function does not explicitly calculate quadrupoles and other π-electronic properties, such that the force field may potentially not adequately model such interactions,[53] although base stacking is described quite well by the force field. (iv) Recently, Paton and Goodman analyzed several MM force field hydrogen bonding parameters[54] and found that they underestimated benchmark interaction energies (they were not strong enough), but the CHARMM force field was not tested by these authors. (v) Finally, we did not introduce counterions to generate an ionic force in the simulations (other than the ones strictly necessary to neutralize the system); this may cause a partial destruction of the secondary structure of the MBDs.[55]

Finally, we believe that the introduction of distance restraints in our simulations is not really detrimental to the conclusions we draw from this work: we apply them to all the MBDs in both their apo and holo forms, so that a comparison between their (relative) dynamics remains sensible; the restraints may have an influence on the global (absolute) dynamics of individual MBDs but so does their insertion into the bundle of six MBDs in vivo.

After session 2, backbone atom coordinate rmsds from initial NMR structures are largest for Mnk1 and smallest for Mnk4 and Mnk6 apo. Further stabilization of the proteins occurs when the metal is bound except for Mnk3 and Mnk5. Mnk2, -4,

and -6 holo are the most stable, with a maximal stability obtained for Mnk4 in perfect agreement with the rmsds observed in the NMR structures of the MBDs.

The stability of the secondary structures was checked with unrestrained MD (session 1). Mnk4 and Mnk6 appear to be very stable in terms of secondary structure. Helix α2 is also very stable in all Mnk systems. In Mnk1 apo, α1, on the other hand, is less stable and several inter β-strand H-bonds disappear during the simulation of Mnk5, meaning that these two MBDs, Mnk1 and Mnk5, probably need, in the complete protein, interactions with other MBDs to stabilize their secondary structures: in the case of Mnk5, this role is probably devoted to Mnk6. In the presence of copper, a stabilization of the secondary structure is observed, especially for Mnk1, but not for Mnk5.

Going back to session 2, in terms of rmsfs, we observe the most dramatic reduction from apo to holo around the MBS in the case of Mnk1. Large rmsfs observed in Mnk5 apo are in agreement with large conformational changes also observed in the fifth domain of Wilson protein WD5 by other authors.[17] Cys1, the first cysteine of the CxxC consensus sequence, which always belongs to loop L1, has a higher rmsf than Cys2. Mnk1 is outstanding in terms of dynamics of the cysteines of its MBS: both cysteines show large fluctuations in their apo form and a large reduction leading to the smallest fluctuations of all MBDs in their holo form.

The side chain of M12 contributes to the stabilization of the protein hydrophobic core except in the case of Mnk3 and Mnk5 in their holo form, where the methionine is solvent-exposed. Rodriguez et al. also observed a large solvent exposure of the methionine in MBD5 apo of the Wilson protein but even more so for MBD3,[17] whereas we see a buried Met13 in the case of Mnk3.

In summary, the fold and general structure of the individual Menkes metal binding domains are similar, but many differences exist in the details of their dynamics. The third metal binding domain, Mnk3, which has the greatest amount of sequence variation (see Figure 1), has some notable differences in the metal binding region but retains the same general fold. The binding of Cu^I leads to an increased level of disorder (rmsf) in the C-terminal half of Mnk3 in opposition with all other Mnks and in good agreement with experimental observation.[26]

In all Mnks except Mnk3, there is a conserved phenylalanine (F66) that lies within the loop adjacent to the cysteines at the MBS. It has been proposed that this hydrophobic residue in the proximity of the binding site stabilizes bound copper.[27,56] In our simulations of Mnk1 and Mnk4, F66 interacts with T13, C17, I21, and M64, in agreement with the results of De Silva et al.,[24] who found that F66 is a key residue in the compact folding of Mnk1 and that its mutation to alanine results in an unfolded structure. We started by studying the exposure of the MBS to the solvent. From our simulations and in agreement with other works, the cysteines of the MBS in their apo form are largely exposed to the solvent, in general (see, for instance, ref 57), with a maximal average exposure for Mnk1. We have outlined unusually high fluctuations of loop L3 in Mnk5 and the role of S37 in other Mnks. Close inspection of our simulations shows that in Mnk1−4, S37 makes a stable hydrogen bond with residue N40 (or E40) and in Mnk6, K41 strongly interacts with E5. Such interactions stabilizing L3 are absent in Mnk5, leaving residue M39 completely solvent-exposed.

Mnk3 contains two phosphorylated residues: T327 (T53), which is phosphorylated only in the presence of an elevated level of copper, and S339 (S65), which is constitutively phosphorylated in a manner independent of copper levels.[58] Recently, Veldhuis et al. suggested, using MD simulations, that S339, which is in a loop facing the copper binding site, may facilitate the copper transfer process by exposing the CxxC copper binding region of MBD3 while copper-induced phosphorylation of T327 would stabilize this change in conformation.[59] In our simulations, Cys1 in Mnk3 apo is indeed largely solvent-exposed while Cys2 is completely buried, but the result is an exposed CxxC motif in Mnk3 holo (high g_H in Table 4). The possibility of a low level of exposure of Cys2 to the solvent is supported by fluorescence labeling experiments by Yatsunyk et al. on the MBDs of the related Wilson protein, showing that the cysteines of MBD3 were the least solvent-exposed.[60]

From our results, Mnk3 and Mnk5 are clearly the MBDs for which the most stable shell of water molecules assembles around the copper. Copper in the MBS is significantly more hydrated in Mnk5 and less hydrated in Mnk1 than in all other Mnks. Moreover, the difference in the maximal g_H of the distributions of water around the sulfur atom of Cys2 between the holo and apo forms of the proteins is maximal for Mnk3 ($\Delta g_H = 0.88 - 0 = 0.88$) and Mnk5 ($\Delta g_H = 1.51 - 0.41 = 1.10$). It is almost zero ($\Delta g_H = 0.90 - 0.88 = 0.02$) in the case of Mnk1. In other words, Cys2 in both Mnk3 and Mnk5 has to go from a hydrophobic environment where it is buried from water to a highly solvent-exposed region upon copper binding. This large thermodynamic change and the fact that Cu^I−water interactions are not favorable[23] could be one explanation for the difficult transfer of Cu^I from HAH1 to Mnk3 or Mnk5 in comparison to Mnk1, for example. Mnk2, Mnk4, and Mnk6 show globally identical radial functions of water around the metal with a bulklike exposure after 7.5 Å. Recently, Gourdon et al. proposed that the six MBD domains arranged in three pairs might appear as two sets of stacked logs with CxxC motifs at their ends.[20] Our results showing a similar water environment around the CxxC motifs of the even-numbered MBDs when Cu^I is bound support this idea.

In the second part of this work, we built model structures of the complexes between HAH1 and the MBDs using standard docking programs. One important factor that affects the quality of the docking prediction is the degree of conformational change of the input structures upon complex formation. Especially important is the degree of such change at the interface area. Comparing the docking results from seven standard programs to the known NMR structure of the complex between HAH1 and Mnk1, we noticed that the programs that perform best are essentially those for which interface residues are given: Haddock, ZDock, and GRAMM-X. Haddock was already used to study the interactions between yeast copper chaperone Atx1 and the first soluble domain of the copper transporting ATPase Ccc2 and showed interactions of an electrostatic nature with hydrogen bonds stabilizing the complex.[61]

The good surprise came from ClusPro, which gave good results (δSS compatible with copper exchange) without any information other than the structures of the isolated proteins, possibly because of its good performance in predicting the structure of oligomeric assemblies from the structures of single subunits.[35]

It has been proposed that the charged surface-exposed residues may contribute to chaperone−target recognition. HAH1 has a considerable positively charged surface region (see HAH1+ in Figure 8) featuring K60 in the proximity of the metal binding loop. Negatively charged regions of several MBDs may be complementary;[56] however, data from our laboratory[45] do not support the idea of electrostatic complementarity being the only driving force for selective HAH1−MBD recognition. Rather, the complementary surface charge distribution may be an important factor in the packing of the MBDs within the N-terminal domain. The observation that the distribution of charges on the surface of MBDs of ATP7A and ATP7B appears to follow the same pattern[15] is consistent with this idea. Our calculations confirmed that electrostatics is the main driving force for the formation of complexes between HAH1 and the MBDs, but the aligned dipole orientation does not lead to the shortest distance between MBS cysteines for copper exchange, especially for Mnk6 (see Table 9). We also showed, in the case of the Mnk1−-HAH1 complex for which a structure exists, that rearrangement of side chains, impossible using rigid body shape complementarity docking programs, was necessary for optimal formation of the complex. Studying the mechanism for the transfer of Cu^I to a construct of the three domains, Mnk4−6, Banci and colleagues showed that the first point of entry for the metal ion into the ATPase is provided by domain 4.[14] Our docking results show that this is presumably so because Mnk4 has a better electrostatic complementarity with respect to the physiological partner and not a better shape complementarity.

The same authors also worked on the effect of copper concentration on its transfer from HAH1 to the complex Mnk1−6.[12] At Cu^IHAH1:Mnk1−6 ratios of up to 3:1, both Mnk1 and Mnk4 formed a metal-mediated adduct with HAH1 whereas Mnk6 (and probably Mnk5) was able to partly remove Cu^I from HAH1. As for the interaction between Mnk3 and HAH1, the transfer of copper(I) from metal-loaded HAH1 was observed experimentally, but the metal distribution was shifted toward binding by HAH1.[26] It was suggested by the same authors that metalation of Mnk3 could be an event suited to signal high intracellular Cu^I concentrations and could trigger the appropriate response(s). In addition, Mnk3 seemed to be the domain that best respects the NMR restraints (smallest restraint violation energy) according to the docking experiments by Banci et al. using Haddock,[19] but these restraints were deduced from the NMR structure of the Mnk1−HAH1 complex. Our Haddock results show a low score for the docking of HAH1 on Mnk3 (see Table 12). On the other hand, in the oriented dipole orientation, the CHARMM interaction energy between Mnk3 and HAH1 is very favorable (see Table 12). In other words, if presented in the "right" orientation, Mnk3 is able to satisfy the distance restraints to HAH1 seen in the Mnk1−HAH1 complex, but this orientation is probably not the most electrostatically favored one or the one adopted in vivo.

In conclusion, let us summarize possible roles of the Menkes MBDs found in the literature and backed up by our modeling study.

The 89-amino acid loop between Mnk1 and Mnk2, if in an extended conformation, could let us think that Mnk1 could act as a copper sensor extending far into the cytoplasm. However, this seems unlikely because the loop mentioned above is systematically predicted to contain a domain, Mnk0, with a ferredoxin fold similar to that of the six identified MBDs (for instance, with JPred[62]). However, Mnk0 does not present any sequence similarity with the MBDs. The loop ranges from P80 to A168 in the Menkes protein sequence and contains only one cysteine, C160; its total charge is 0, and its electric dipole is 167 D (using the CHARMM19 force field). A quick structural model of Mnk0 was built by homology with Mnk1−6 (not shown) from V83 to K155. Then a model structure of the complex between Mnk0 and Mnk1 was built with the different docking programs used above. Most programs yield a structure of the complex compatible with a simultaneous docking between Mnk1 and HAH1 (no steric clash between Mnk0 and HAH1). Results from GRAMM-X, for instance, suggest an interface between Mnk1 and Mnk0 composed of residues D67, I70, and H71 in Mnk1 and residues N135, A136, and N137, part of Mnk0, in ATP7A. An interesting suggestion of this model is the stabilization of the C-terminal part of Mnk1 (see Figure 4) via interaction with Mnk0; Mnk1 would thus be part of the bundle of all MBDs, probably interacting with Mnk0. As a general trend, we believe that polarity of the MBDs is most important for their packing inside the bundle and, in second, for their interactions with HAH1.

We already noticed the high proportion of serine residues in Mnk3. If we include the loop between Mnk3 and Mnk4, we have 23 serine residues between N275 and P374 (23%), including eight phosphorylation sites clustered in a 24-residue serine-rich region between S339 and S362.[58] It has been suggested that phosphorylation in this region may regulate the copper translocating activity in the catalytic cycle as observed for the yeast copper-ATPase Ccc2.[63] Clearly, we did not investigate this possible role of Mnk3 in this work but confirmed its poor interaction with HAH1 with our docking results and showed a complex rearrangement of the amino acid side chains around Cys2 necessary and probably energetically unfavored before copper binding.

As already noticed, Mnk1 and Mnk4 are both followed by long loops connecting them to the next MBD: 89 amino acids between Mnk1 and Mnk2 and 39 amino acids between Mnk4 and Mnk5. This probably facilitates their interaction with HAH1 without affecting their stability in the bundle of MBDs. Mnk4 presents the largest total charge and electric dipole moment of all MBDs and also an excellent stability with the lowest value of its rmsd during dynamics (session 2). The facilitated transfer of copper from HAH1 to Mnk4 was shown experimentally[14] and confirmed by our docking simulations yielding a very good docking score between the two partners. Mnk4 and Mnk1 seem to behave similarly from structural, dynamical, and electrostatic points of view.

Mnk5 presents a high mobility and large fluctuations in its holo form. It appears similar to Mnk2 in the way it docks to HAH1 and is able to receive copper from the chaperone. Large fluctuations of MBS loop L1 in the presence of copper, reinforced by interactions with the largely fluctuating loop L3, may have a role in the transfer of copper from and to Mnk5.

An important result of this work is the apparent direct correlation between the difference in the fluctuations of the MBS loop in its apo and holo forms and the measured affinity of the MBD for copper. The copper binding affinities of the Menkes MBDs (except Mnk4) were recently determined by Banci's group.[64] The results mostly corroborate their previous data with affinities of Mnk1 (2.9 fM), Mnk2 (4.9 fM), and Mnk6 (2.6 fM) 3−7 times higher than that of HAH1, similar to that of HAH1 for Mnk5 (13 fM), and much lower in the case of Mnk3 (104 fM). The difference in fluctuations of the MBS loop

that we measure decreases from Mnk1 to Mnk6, Mnk4, and Mnk2, in very good agreement with the affinity scale (proposed above) obtained from mass spectrometry experiments, provided that this technique can give a quantitative value of these affinities.

We have no clear interpretation concerning the role of Mnk2. More work is probably needed to exactly understand the packing and role of each MBD. Awaiting a crystal or NMR structure of this bundle of MBDs, we have several ideas for future theoretical work in the field. Awaiting a confirmation of the ferredoxin fold of Mnk0 through a NMR structure, we should be able to predict the structure of Mnk0−6, including the non-copper binding domain Mnk0 using the NMR structures of the six individual MBDs and also the NMR structures of the pairs of closely related Wilson protein MBDs: Wls3−4[65] and Wls5−6.[66] Coarse-grained models of the MBDs could be built and associated using long MD simulations.

Gourdon and colleagues discovered a platform in the protein LpCopA, a P1B-type ATPase from the bacterium *L. pneumophila*, with positive charges around the putative entry site for copper, providing an ideal docking surface for a negatively charged copper donor.[67] This copper donor may well be a MBD in the case of the Menkes protein. The authors of the structure of LpCopA could not clarify this issue because LpCopA bears only one MBD and because the mobility of this domain prevented them from obtaining its fully resolved structure.[9] Gourdon et al. proposed in their paper on LpCopA that helices MB′ (W131−T143) and M1 (M148−W169) form a platform that may be part of the Cu^{I} entry pathway. The equivalent mostly conserved residues in ATP7A range from W729 to H741 and from M746 to V767 for MB′ and M1, respectively. In this work, Mnk6 was docked to the ATP7A core in the region above the platform. Among the three candidate residues proposed by the same authors for initial Cu^{I} coordination, M148 in M1 (M746 is the equivalent), E205 in M2 (E798 is the equivalent), and D337 in M3 (D935 is the equivalent), we chose the most solvent-exposed, namely E798, to direct our docking.

In their following paper,[20] Gourdon et al. suggest another position for Mnk6 that we have analyzed as the GourdMod model. They claim that Mnk6 may be repulsed by the positive charges on the MB platform. In our Haddock model, the +1 charge residues K737 and K742 form stabilizing interactions with N40 (N602) and E66 (E628), respectively. Moreover, Mnk6 in its holo form bears a negative total charge of −1 (see Table 7). We can say that because of the distance between Cu^{I} and the proposed channel entry for the metal in ATP7A, Gourdon et al. rule out the possibility of direct transfer of Cu^{I} from Mnk6. On the contrary, we have based our alternative model on the hypothesis of this direct transfer and have seen that the resulting structure had a good energy and a positioning of Mnk6 compatible with the binding of Mnk5 and preceding MBDs.

We do not mean that metallochaperone HAH1 is not implied in the transfer of Cu^{I} to ATP7A: HAH1 bears the same charge as Mnk6, and ongoing simulations tend to show that HAH1 is indeed able to bind to the ATPase platform in a conformation close to that of Mnk6 presented here.

The MD simulations and docking results presented here, based on simple molecular mechanics force fields, give good insight into the reasons why the transfer of copper preferentially occurs from HAH1 to Mnk1 or Mnk4. From a theoretical perspective, it might be interesting to devise a new system-dependent docking protocol with CHARMM that would lower the contribution of electrostatics to the total interaction energy between partners and thus constitute a good docking tool with a sensible docking score.

We might as well use an electronic description of the MBS and especially the copper ion.[57] A quantum mechanics/molecular mechanics-type treatment of the MBS could be used to study the influence of the different amino acids surrounding the MBS on the stability of the apo and holo structures of the MBDs.

To clarify the possible competition between the MBDs and HAH1 for the transfer of copper to the ATPase core, we propose to run long detailed simulations in which we insert the ATP7A model inside a lipid membrane and test the stability of Mnk6 and HAH1 at the platform entry with either a molecular mechanics or quantum mechanics treatment of the metal.

■ ASSOCIATED CONTENT

Ⓢ Supporting Information

Backbone atom coordinate rmsd from initial NMR structures during MD simulations for apo Mnk models (session 1) (Figure S1), apo Mnk models (session 2) (Figure S2), holo Mnk models (session 1) (Figure S3), and holo Mnk models (session 2) (Figure S4), evolution of secondary structure elements of Mnk6 apo with time (session 1) (Figure S5), the number of residues in each type of secondary structure for apo Mnk systems as calculated with Stride for NMR- and MD-averaged structures (Table S1), the same for holo Mnk systems (Table S2), radial distribution function of water around methionine for all apo Mnk systems (Figure S6), and average distances (and S−Cu^{I}−S angles) between copper and heavy atoms close to the metal binding site for all holo forms of Menkes MBDs (Table S3). This material is available free of charge via the Internet at http://pubs.acs.org.

■ AUTHOR INFORMATION

Corresponding Author

*Telephone: (33)0438782963. Fax: (33)0438785487. E-mail: serge.crouzy@cea.fr.

Present Address

§Centre de Recherche Public de la Santé 84, Val Fleuri L-1536, Luxembourg.

Funding

K.A. was supported by a grant from Direction Internationale du CEA.

Notes

The authors declare no competing financial interest.

■ ABBREVIATIONS

MBD, metal binding domain; MBS, metal binding site; MD, molecular dynamics; rmsd, root-mean-square deviation; rmsf, root-mean-square fluctuation; ABNR, adopted basis Newton−Raphson.

■ REFERENCES

(1) Arguello, J. M., Eren, E., and Gonzalez-Guerrero, M. (2007) The structure and function of heavy metal transport P1B-ATPases. *BioMetals 20*, 233−248.

(2) Petris, M. J., Strausak, D., and Mercer, J. F. (2000) The Menkes copper transporter is required for the activation of tyrosinase. *Hum. Mol. Genet. 9*, 2845−2851.

(3) Steveson, T. C., Ciccotosto, G. D., Ma, X. M., Mueller, G. P., Mains, R. E., and Eipper, B. A. (2003) Menkes protein contributes to the function of peptidylglycine α-amidating monooxygenase. *Endocrinology 144*, 188−200.
(4) Tchaparian, E. H., Uriu-Adams, J. Y., Keen, C. L., Mitchell, A. E., and Rucker, R. B. (2000) Lysyl oxidase and P-ATPase-7A expression during embryonic development in the rat. *Arch. Biochem. Biophys. 379*, 71−77.
(5) Qin, Z., Itoh, S., Jeney, V., Ushio-Fukai, M., and Fukai, T. (2006) Essential role for the Menkes ATPase in activation of extracellular superoxide dismutase: Implication for vascular oxidative stress. *FASEB J. 20*, 334−336.
(6) Monty, J. F., Llanos, R. M., Mercer, J. F., and Kramer, D. R. (2005) Copper exposure induces trafficking of the menkes protein in intestinal epithelium of ATP7A transgenic mice. *J. Nutr. 135*, 2762−2766.
(7) Royce, P. M., and Steinmann, B. (1990) Markedly reduced activity of lysyl oxidase in skin and aorta from a patient with Menkes' disease showing unusually severe connective tissue manifestations. *Pediatr. Res. 28*, 137−141.
(8) Lutsenko, S., LeShane, E. S., and Shinde, U. (2007) Biochemical basis of regulation of human copper-transporting ATPases. *Arch. Biochem. Biophys. 463*, 134−148.
(9) Gourdon, P., Liu, X. Y., Skjorringe, T., Morth, J. P., Muller, L. B., Pedersen, B. P., and Nissen, P. (2011) Crystal structure of a copper-transporting PIB-type ATPase. *Nature 475*, 59−64.
(10) Payne, A. S., and Gitlin, J. D. (1998) Functional expression of the menkes disease protein reveals common biochemical mechanisms among the copper-transporting P-type ATPases. *J. Biol. Chem. 273*, 3765−3770.
(11) Cater, M. A., Forbes, J., La Fontaine, S., Cox, D., and Mercer, J. F. (2004) Intracellular trafficking of the human Wilson protein: The role of the six N-terminal metal-binding sites. *Biochem. J. 380*, 805−813.
(12) Banci, L., Bertini, I., Cantini, F., Della-Malva, N., Migliardi, M., and Rosato, A. (2007) The different intermolecular interactions of the soluble copper-binding domains of the menkes protein, ATP7A. *J. Biol. Chem. 282*, 23140−23146.
(13) Strausak, D., La Fontaine, S., Hill, J., Firth, S. D., Lockhart, P. J., and Mercer, J. F. (1999) The role of GMXCXXC metal binding sites in the copper-induced redistribution of the Menkes protein. *J. Biol. Chem. 274*, 11170−11177.
(14) Banci, L., Bertini, I., Cantini, F., Chasapis, C. T., Hadjiliadis, N., and Rosato, A. (2005) A NMR study of the interaction of a three-domain construct of ATP7A with copper(I) and copper(I)-HAH1: The interplay of domains. *J. Biol. Chem. 280*, 38259−38263.
(15) Huffman, D. L., and O'Halloran, T. V. (2001) Function, structure, and mechanism of intracellular copper trafficking proteins. *Annu. Rev. Biochem. 70*, 677−701.
(16) Banci, L., Bertini, I., Ciofi-Baffoni, S., Chasapis, C. T., Hadjiliadis, N., and Rosato, A. (2005) An NMR study of the interaction between the human copper(I) chaperone and the second and fifth metal-binding domains of the Menkes protein. *FEBS J. 272*, 865−871.
(17) Rodriguez-Granillo, A., Crespo, A., and Wittung-Stafshede, P. (2009) Conformational dynamics of metal-binding domains in Wilson disease protein: Molecular insights into selective copper transfer. *Biochemistry 48*, 5849−5863.
(18) Poger, D., Fuchs, J. F., Nedev, H., Ferrand, M., and Crouzy, S. (2005) Molecular dynamics study of the metallochaperone Hah1 in its apo and Cu(I)-loaded states: Role of the conserved residue M10. *FEBS Lett. 579*, 5287−5292.
(19) Banci, L., Bertini, I., Calderone, V., Della-Malva, N., Felli, I. C., Neri, S., Pavelkova, A., and Rosato, A. (2009) Copper(I)-mediated protein-protein interactions result from suboptimal interaction surfaces. *Biochem. J. 422*, 37−42.
(20) Gourdon, P., Sitsel, O., Karlsen, J. L., Møller, L. B., and Nissen, P. (2012) Structural models of the human copper P-type ATPases ATP7A and ATP7B. *Biol. Chem. 393*, 205−216.
(21) Brooks, B. R., Bruccoleri, R. E., Olafson, B. D., States, D. J., Swaminathan, S., and Karplus, M. (1983) CHARMM: A program for macromolecular energy, minimization, and dynamics calculations. *J. Comput. Chem. 4*, 187−217.
(22) Feller, S., and MacKerell, A. D. (2000) An Improved Empirical Potential Energy Function for Molecular Simulations of Phospholipids. *J. Phys. Chem. B 104*, 7510−7515.
(23) Fuchs, J. F., Nedev, H., Poger, D., Ferrand, M., Brenner, V., Dognon, J. P., and Crouzy, S. (2006) New model potentials for sulfur-copper(I) and sulfur-mercury(II) interactions in proteins: From ab initio to molecular dynamics. *J. Comput. Chem. 27*, 837−856.
(24) DeSilva, T. M., Veglia, G., and Opella, S. J. (2005) Solution structures of the reduced and Cu(I) bound forms of the first metal binding sequence of ATP7A associated with Menkes disease. *Proteins 61*, 1038−1049.
(25) Banci, L., Bertini, I., Del Conte, R., D'Onofrio, M., and Rosato, A. (2004) Solution structure and backbone dynamics of the Cu(I) and apo forms of the second metal-binding domain of the Menkes protein ATP7A. *Biochemistry 43*, 3396−3403.
(26) Banci, L., Bertini, I., Cantini, F., DellaMalva, N., Herrmann, T., Rosato, A., and Wüthrich, K. (2006) Solution structure and intermolecular interactions of the third metal-binding domain of ATP7A, the Menkes disease protein. *J. Biol. Chem. 281*, 29141−29147.
(27) Gitschier, J., Moffat, B., Reilly, D., Wood, W. I., and Fairbrother, W. J. (1998) Solution structure of the fourth metal-binding domain from the Menkes copper-transporting ATPase. *Nat. Struct. Biol. 5*, 47−54.
(28) Banci, L., Bertini, I., Cantini, F., Migliardi, M., Rosato, A., and Wang, S. (2005) An atomic-level investigation of the disease-causing A629P mutant of the Menkes protein, ATP7A. *J. Mol. Biol. 352*, 409−417.
(29) Jorgensen, W. L., Chandrasekhar, J., and Madura, J. D. (1983) Comparison of simple potential functions for simulating liquid water. *J. Chem. Phys. 79* (2), 926−935.
(30) Darden, T. A., York, D. M., and Pedersen, L. G. (1993) Particle mesh Ewald: An *N*-log(*N*) method for Ewald sums in large systems. *J. Chem. Phys. 98*, 10089−10092.
(31) Ryckaert, J.-P., Ciccotti, G., and Berendsen, H. J. C. (1977) Numerical integration of the Cartesian equations of motion of a system with constraints: Molecular dynamics of *n*-alkanes. *J. Comput. Phys. 23*, 327−341.
(32) Portnoy, M. E., Rosenzweig, A. C., Rae, T., Huffman, D. L., O'Halloran, T. V., and Culotta, V. C. (1999) Structure-function analyses of the ATX1 metallochaperone. *J. Biol. Chem. 274*, 15041−15045.
(33) de Vries, S. J., van Dijk, M., and Bonvin, A. M. (2010) The HADDOCK web server for data-driven biomolecular docking. *Nat. Protoc. 5*, 883−897.
(34) Ritchie, D. W., and Kemp, G. J. (2000) Protein docking using spherical polar Fourier correlations. *Proteins 39*, 178−194.
(35) Kozakov, D., Hall, D. R., Beglov, D., Brenke, R., Comeau, S. R., Shen, Y., Li, K., Zheng, J., Vakili, P., Paschalidis, I. C. h., and Vajda, S. (2010) Achieving reliability and high accuracy in automated protein docking: ClusPro, PIPER, SDU, and stability analysis in CAPRI rounds 13−19. *Proteins 78*, 3124−3130.
(36) Pierce, B. G., Hourai, Y., and Weng, Z. (2011) Accelerating protein docking in ZDOCK using an advanced 3D convolution library. *PLoS One 6*, e24657.
(37) Zacharias, M. (2005) ATTRACT: Protein-protein docking in CAPRI using a reduced protein model. *Proteins 60*, 252−256.
(38) Duhovny, D., Nussinov, R., and Wolfson, H. J. (2002) Efficient Unbound Docking of Rigid Molecules. Proceedings of the second Workshop on Algorithms in Bioinformatics (WABI) Rome, Italy, Lecture Notes in Computer Science 2452, pp 185−200, Springer-Verlag.
(39) Tovchigrechko, A., and Vakser, I. A. (2006) GRAMM-X public web server for protein-protein docking. *Nucleic Acids Res. 34*, W310−W314.

(40) Thompson, J. D., Higgins, D. G., and Gibson, T. J. (1994) CLUSTAL W: Improving the sensitivity of progressive multiple sequence alignment through sequence weighting, position-specific gap penalties and weight matrix choice. *Nucleic Acids Res. 22*, 4673−4680.
(41) Beitz, E. (2000) TEXshade: Shading and labeling of multiple sequence alignments using LATEX2 epsilon. *Bioinformatics 16*, 135−139.
(42) Feig, M., Karanicolas, J., and Brooks, C. L. (2004) MMTSB Tool Set: Enhanced sampling and multiscale modeling methods for applications in structural biology. *J. Mol. Graphics Modell. 22*, 377−395.
(43) Frishman, D., and Argos, P. (1995) Knowledge-based protein secondary structure assignment. *Proteins 23*, 566−579.
(44) Humphrey, W., Dalke, A., and Schulten, K. (1996) VMD: Visual molecular dynamics. *J. Mol. Graphics 14*, 33−38.
(45) Morin, I., Cuillel, M., Lowe, J., Crouzy, S., Guillain, F., and Mintz, E. (2005) Cd^{2+}- or Hg^{2+}-binding proteins can replace the Cu^{+}-chaperone Atx1 in delivering Cu^{+} to the secretory pathway in yeast. *FEBS Lett. 579*, 1117−1123.
(46) Baker, N. A., Sept, D., Joseph, S., Holst, M. J., and McCammon, J. A. (2001) Electrostatics of nanosystems: Application to microtubules and the ribosome. *Proc. Natl. Acad. Sci. U.S.A. 98*, 10037−10041.
(47) Lazaridis, T., and Karplus, M. (1999) Effective energy function for proteins in solution. *Proteins 35*, 133−152.
(48) Larin, D., Mekios, C., Das, K., Ross, B., Yang, A. S., and Gilliam, T. C. (1999) Characterization of the interaction between the Wilson and Menkes disease proteins and the cytoplasmic copper chaperone, HAH1p. *J. Biol. Chem. 274*, 28497−28504.
(49) Strausak, D., Howie, M. K., Firth, S. D., Schlicksupp, A., Pipkorn, R., Multhaup, G., and Mercer, J. F. (2003) Kinetic analysis of the interaction of the copper chaperone Atox1 with the metal binding sites of the Menkes protein. *J. Biol. Chem. 278*, 20821−20827.
(50) Myers, J. K., and Pace, C. N. (1996) Hydrogen bonding stabilizes globular proteins. *Biophys. J. 71*, 2033−2039.
(51) Pan, A. C., Cuello, L. G., Perozo, E., and Roux, B. (2011) Thermodynamic coupling between activation and inactivation gating in potassium channels revealed by free energy molecular dynamics simulations. *J. Gen. Physiol. 138*, 571−580.
(52) Mackerell, A. D., Feig, M., and Brooks, C. L. (2004) Extending the treatment of backbone energetics in protein force fields: Limitations of gas-phase quantum mechanics in reproducing protein conformational distributions in molecular dynamics simulations. *J. Comput. Chem. 25*, 1400−1415.
(53) Macias, A. T., and Mackerell, A. D. (2005) CH/π interactions involving aromatic amino acids: Refinement of the CHARMM tryptophan force field. *J. Comput. Chem. 26*, 1452−1463.
(54) Paton, R. S., and Goodman, J. M. (2009) Hydrogen Bonding and π-Stacking: How Reliable are Force Fields? A Critical Evaluation of Force Field Descriptions of Nonbonded Interactions. *J. Chem. Inf. Model. 49* (4), 944−955.
(55) Ibragimova, G. T., and Wade, R. C. (1998) Importance of explicit salt ions for protein stability in molecular dynamics simulation. *Biophys. J. 74*, 2906−2911.
(56) Walker, J. M., Huster, D., Ralle, M., Morgan, C. T., Blackburn, N. J., and Lutsenko, S. (2004) The N-terminal metal-binding site 2 of the Wilson's Disease Protein plays a key role in the transfer of copper from Atox1. *J. Biol. Chem. 279*, 15376−15384.
(57) Op't Holt, B. T., and Merz, K. M. (2007) Insights into Cu(I) exchange in HAH1 using quantum mechanical and molecular simulations. *Biochemistry 46*, 8816−8826.
(58) Veldhuis, N. A., Valova, V. A., Gaeth, A. P., Palstra, N., Hannan, K. M., Michell, B. J., Kelly, L. E., Jennings, I., Kemp, B. E., Pearson, R. B., Robinson, P. J., and Camakaris, J. (2009) Phosphorylation regulates copper-responsive trafficking of the Menkes copper transporting P-type ATPase. *Int. J. Biochem. Cell Biol. 41*, 2403−2412.
(59) Veldhuis, N. A., Kuiper, M. J., Dobson, R. C., Pearson, R. B., and Camakaris, J. (2011) In silico modeling of the Menkes copper-translocating P-type ATPase 3rd metal binding domain predicts that phosphorylation regulates copper-binding. *BioMetals 24*, 477−487.
(60) Yatsunyk, L. A., and Rosenzweig, A. C. (2007) Cu(I) binding and transfer by the N terminus of the Wilson disease protein. *J. Biol. Chem. 282*, 8622−8631.
(61) Arnesano, F., Banci, L., Bertini, I., and Bonvin, A. M. (2004) A docking approach to the study of copper trafficking proteins; interaction between metallochaperones and soluble domains of copper ATPases. *Structure 12*, 669−676.
(62) Cole, C., Barber, J. D., and Barton, G. J. (2008) The Jpred 3 secondary structure prediction server. *Nucleic Acids Res. 36*, 197−201.
(63) Valverde, R. H., Morin, I., Lowe, J., Mintz, E., Cuillel, M., and Vieyra, A. (2008) Cyclic AMP-dependent protein kinase controls energy interconversion during the catalytic cycle of the yeast copper-ATPase. *FEBS Lett. 582*, 891−895.
(64) Banci, L., Bertini, I., Ciofi-Baffoni, S., Kozyreva, T., Zovo, K., and Palumaa, P. (2010) Affinity gradients drive copper to cellular destinations. *Nature 465*, 645−648.
(65) Banci, L., Bertini, I., Cantini, F., Rosenzweig, A. C., and Yatsunyk, L. A. (2008) Metal binding domains 3 and 4 of the Wilson disease protein: Solution structure and interaction with the copper(I) chaperone HAH1. *Biochemistry 47*, 7423−7429.
(66) Achila, D., Banci, L., Bertini, I., Bunce, J., Ciofi-Baffoni, S., and Huffman, D. L. (2006) Structure of human Wilson protein domains 5 and 6 and their interplay with domain 4 and the copper chaperone HAH1 in copper uptake. *Proc. Natl. Acad. Sci. U.S.A. 103*, 5729−5734.
(67) Robinson, N. J. (2011) Structural biology: A platform for copper pumps. *Nature 475*, 41−42.